Received 9 July 2021; accepted 15 July 2021. Date of publication 26 July 2021; date of current version 6 August 2021.

Digital Object Identifier 10.1109/OJCOMS.2021.3099524

Characterization and Exploitation of Quasi Determinism in Multi-Conductor Power Line Communication Noise

DAVIDE RIGHINI (Student Member, IEEE), AND ANDREA M. TONELLO (Senior Member, IEEE)

Department of Networked and Embedded Systems, University of Klagenfurt, 9020 Klagenfurt, Austria

CORRESPONDING AUTHOR: D. RIGHINI (e-mail: davide.righini@aau.at)

ABSTRACT Several experiments and field trials have shown that deterministic components characterize the Power Line Communication (PLC) noise across multiple-conductors. This article aims at understanding the main origins of these noise components and evaluate several methods to characterize them statistically. The correlation, distance-correlation, mutual information estimation, and a proposed linear coefficient ratio, are used to analyze the noise time-series statistically. The analysis of the PLC noise deterministic components allow us to develop an enhanced noise model that includes them. The presence of deterministic noise fosters the development of coding and decoding algorithms that aim at mitigating the noise effect. New decoding techniques called Quasi-Deterministic-Decoding are detailed and tested with single-input-multiple-output (SIMO) 1x2 and multiple-input-multiple-output (MIMO) 2x2 transmission configurations using real PLC noise and channel realizations. The proposed model leads to a better representation of the PLC noise traces and, consequently, the development of improved coding algorithms for reliable data transmission at low signal-to-noise ratios.

INDEX TERMS Noise, noise mitigation, MIMO, space-time coding, space-time processing, power line communications.

I. INTRODUCTION

THE TELECOMMUNICATION industry is continuously demanding higher data-rates and improved network performance. Power Line Communication (PLC) is a relevant technology that supports hyper-connectivity and ubiquitous coverage [1].

PLC has experienced an increase in deployment [2], and for applications such as Home Automation, Smart Grid control, Power Grid Monitoring, it provides several advantages [2], [3]. Nonetheless, the Power Line Network (PLN) is not designed for communication purposes. Moreover, it is challenged by harsh noise [4]–[7].

The presence of noise in PLNs significantly affects PLC's performance and its recently explored applications, e.g., diagnostics, cable fault detection [8], [9], enhanced communication techniques such as multiple-input-multiple-output (MIMO) [10] and in-band full duplex [11], [12]. Noise during diagnostic measurements may cause wrong readings and thus a wrong prediction of the power line status. Indirect measurement techniques, such as impedance estimation for fault detection, are significantly affected by noise [13], [14]. Noise spatial correlation or dependency may affect the performance of MIMO PLC, reducing the throughput gain provided by the multi-channel system. In-band full-duplex is also an upcoming technology for PLC, where signals are sent and received simultaneously, exploiting the same frequency band. Noise reduction techniques are crucial for accurate self-interference estimation and cancellation, enabling the implementation of in-band full-duplex technology successfully.

In the literature, the PLC noise has been analyzed spatially, spectrally, and temporally. An analysis of the noise measured at the source was done in [7] and at the receiver in [15]. Spectral analysis of the noise measured in the Narrow-Band spectrum (10-1000kHz) was done in [16], [17], and concerning the Broad-Band spectrum (1 - 100MHz) was described in [7], [10]. A temporal analysis of the noise measured with Digital Storage Oscilloscopes (DSOs) was done in [18].

Two approaches are then possible for noise characterization and modeling: bottom-up and top-down. With the bottom-up approach, noise models are derived by studying the source that generates them. Parametric models are built and fit based on experience and simulations [15], [19]. Whereas, with the top-down approach, the noise characteristics and models are extracted by applying reverse engineering techniques on the entire noise dataset. Phenomenological data analysis is endured by statistical models and big data analytics techniques, such as automatic clustering and neural-network tools [20], [21].

In more detail, both top-down and bottom-up approaches have been exploited to characterize the Single-Input-Single-Output (SISO) PLC noise. The idea of noise as the sum of multiple components has been presented in [22]. Then, Zimmerman and Dostert defined five conventional noise classes [18]. The Colored Background Noise (CBGN) class exhibits a stationary behavior [23], [24], associated with Normal and Alpha Stable distributions [25]. The Narrow-Band Noise (NBN) class models the noise as a sum of different independent harmonic interferences [26], [27]. Periodic Impulsive Noise Synchronous to mains (PINS) and Periodic Impulsive Noise Asynchronous to mains (PINAS) are described with similar models by a summation of different independent Gaussian components with a time-varying power [23], [24]. The Aperiodic Impulsive Noise (APIN) exhibits no deterministic behavior, and it is usually described with a Middleton Class A model [19], [28].

The top-down approach has been exploited in the literature to statistically analyze the Probability Density Functions (PDFs) of the PLC noise realizations. The MIMO PLC channel and related noise have been initially measured and studied by the ETSI STF410 working group and led to a MIMO broadband noise model that accounts for the frequency and spatial correlation [5]. The spatial noise correlation between different outlets has been considered in [5]. Moreover, the correlation and determinism between conductors have been highlighted in [29].

The above-listed endeavors considered the noise as a stochastic process that comprises multiple components with different characteristics. However, only recently, it has been noticed that relevant parts of the PLC noise often assume predictable behaviors that, in some cases, can be considered as deterministic [29]. Such a behavior has been observed among noise traces acquired over multi-conductors (MCOs). Besides, in [25], the correlation and the distance-correlation metric have been exploited to identify noise classes and dependencies automatically. However, a comprehensive analysis and a model of the deterministic noise (DN) component are missing. This paper aims at filling this gap, mainly focusing on the noise model for the MIMO transmission systems. Four main contributions are given:

A) An analysis of the MIMO PLC noise and its relation to the MIMO channel transfer function and line impedance. This article provides a methodology to study the MIMO front-end circuits and the coupling of noise sources. Specifically for three conductors systems (i.e., the most common medium available for indoor PLC), a detailed schematic and model is studied to clarify the relationships between noise, channel transfer function, and line impedances.

B) A network/circuit analysis to explain the origin of noise coupling and determinism. The PLC network's physical characteristics influence noise propagation. The proposed analysis identifies the reasons that cause the noise's deterministic effects through a circuital description of the PLN and components.

C) Metrics to infer determinism. A straightforward method to identify deterministic behaviors from a noise signal is not available in the literature. In this paper, an analysis of real data is performed to identify and characterize the MCO noise determinism. Several known metrics, such as cross-correlation, distance correlation, and mutual information, are considered and compared. Moreover, we introduce the linear coefficient ratio to characterize the linear dependencies.

D) Simple coding and decoding algorithms for both single-input-multiple-output (SIMO) and MIMO PLC transmission in the presence of MCO noise determinism. The noise model's knowledge, and precisely its quasi deterministic (QD) behavior, have been exploited to devise new decoding algorithms for both SIMO and MIMO transmission systems. The process to estimate the parameter β, that models the deterministic relation between MCO noise traces is explained and tested through a simulated PLC MIMO 2x2 system that exploits a dataset of measured noise and channel-transfer-functions (CTFs). The proposed noise mitigation algorithms aim to remove the DN component from the received signal. It has been shown that the prosed techniques allow achieving good decoding results, w.r.t. the typically described methods.

The paper is organized as follows. The state of the art on PLC noise classes is summarized in Section II. Section III describes the relation between CTFs, line impedances, and noise sources, while Section IV, summarizes the metrics to detect the noise determinism. In Section V, the experimental evidence has been discussed. Successively, in Section VI, a new model that includes the DN component is proposed. In Section VII, new decoding techniques that exploit the proposed noise model are detailed and evaluated. Then, the conclusion follows in Section VIII. Eventually, in the Appendix, the noise measurement techniques and the acquired datasets are detailed.

II. NOISE CLASSIFICATION

Noise sources are modeled as voltage generators located at loads of the PLN, and as radiative sources of electromagnetic signals located in the network's surroundings. Radiated electromagnetic waves are captured by the PLC network and propagated through the network branches. Power lines are susceptible to these phenomena for several reasons:

- no shields are installed on the cables; thus, electromagnetic waves are easily coupled to the PLN;
- impedance mismatches between loads and the network impedance cause radiation at the interconnections [30];

- the transmission line non-ideal effects cause signal conversions along the network (i.e., from the differential to the common mode and vice versa) [31].

Therefore, the PLC noise at the receiver outlet is too complex to be described with a simple mathematical model since several physical phenomena cause it. A way forward is to consider it as the sum of six voltage components (CBGN, NBN, PINS, PINAS, APIN, DN) [18], [29]:

$$v(t) = v^{(\mathrm{CBGN})}(t) + v^{(\mathrm{NBN})}(t) + v^{(\mathrm{PINS})}(t) + \\ + v^{(\mathrm{PINAS})}(t) + v^{(\mathrm{APIN})}(t) + v^{(\mathrm{DN})}(t). \quad (1)$$

These noise components have been identified in both single and MCO PLC systems. The external noise sources do not depend on the type of communication medium. However, the cable geometries and electrical characteristics, loads, and devices connected to the PLN might change the noise signal in the path between the noise source and the PLC outlet, where the noise is acquired. Moreover, the PLC hardware designed for single-conductor is different from the one that exploits MCOs since different couplers and front-ends are used. Therefore, also the PLN response is different, and this can affect the noise signal. Moreover, the MCOs interact with each other through cross-talk effects. Therefore, both signal and noise can be affected by this coupling effect.

A. CLASSIFICATION AND GENERATION METHODS

The PLC noise characterization is a tedious and time-consuming activity because of the variegated nature of the signal. Such an effort has been documented in several papers. Mostly empirical methods have been applied to identify the main classes of noise. Then, theoretical methods such as statistical fitting have been applied to define the main noise classes' characteristics through customized probability density functions.

With large data sets, big data analytics turn out to be useful. The article [25] offers an example of the effectiveness of this approach applied to the PLC noise. An automatic procedure to classify the PLC noise has produced similar results as the traditional noise classification. The noise traces have been analyzed according to many features such as voltage peaks, energy, mean value, central moments, and estimated entropy. For each noise trace segment (windowed time series), the features mentioned above have been computed and collected in an organized dataset. Then a clustering technique has been used to identify the main noise classes.

Another possible variation of the noise classification is to explore machine learning techniques to extract the noise features and separate the noise phenomena. In [21], a machine learning technique used this approach to preprocess a dataset of measured time series to generate new noise time-series that follow the same statistics of the measured ones. The idea is to train a neural-network to project the noise time series in an appropriate latent space where the features can be extracted and used to classify the noise. In general, the exploitation of machine learning techniques can consistently aid the process of classification and the detection of noise classes in real noise scenarios [20], [32].

B. THE DETERMINISTIC NOISE

The noise in a MCO power line, in addition to the classes mentioned earlier, may manifest similar characteristics between different conductor pairs. An example is the high spatial correlation between the cyclostationary noise signals on different line phases, usually caused by network-based switched power supplies [32]. Moreover, measurements demonstrate that MCO noise is not only correlated but sometimes reveals deterministic behaviors [29]. In general, the noise can be written as a sum of deterministic ($v^{(\mathrm{DN})}(t)$) and stochastic ($v^{(\mathrm{SN})}(t)$) voltage components:

$$v(t) = v^{(\mathrm{DN})}(t) + v^{(\mathrm{SN})}(t). \quad (2)$$

A noise realization is said deterministic when the DN component is much higher than the stochastic one (SN). Otherwise, it is considered stochastic. As shown in (3), the DN is defined as a deterministic function $\mathcal{F}$ between measurable quantities (i.e., other noise traces $v_j^{(n)}$ with $j \neq k$, and indexes $j, k \in \{1, 2, \dots\}$; channel impulse responses h; load impedances z_L) that characterize the transmission system.

$$v_k^{(\mathrm{DN})}(t) = \mathcal{F}\big[v_j(t), h, z_L\big]. \quad (3)$$

The SN behavior is well characterized in the literature. Therefore, only the deterministic phenomena are discussed in this paper. Specifically, four types of determinism have been identified in the PLC noise: MCO, location, temporal, and spectral.

- MCO DN may exist in PLN with $c \geq 3$ conductors. This noise class represents the deterministic relations between noise voltage signals at different conductors of the same cable termination:

$$v_k^{(\mathrm{DN})}(t) = \mathcal{F}_{\mathrm{a}}\big[v_j(t)\big], \quad (4)$$

  where v_j represents the noise trace measured at the j-th conductor of the local node (i.e., the noise measured at the k-th conductor depends deterministically from the noise on the adjacent j-th conductor). This noise is mostly caused by radiated noise coupled to the adjacent cable and non-ideal signal mode conversion (i.e., from differential to common mode).
- Location DN represents the deterministic relation between noise realizations at different outlets of the PLC network:

$$v_k^{(\mathrm{DN})}(t) = \mathcal{F}_{\mathrm{b}}\big[v_j(t), h_{kj}\big]. \quad (5)$$

  In Eq. (5) the subscripts j and k represent different outlets of the PLN. Typically such outlets are located with at least one meter distance from each other. This type of noise is primarily caused by the topological structure of the PLN. When a strong noise signal propagates through a common branch of a mesh network, this noise is visible at multiple outlets. Therefore, the

relation between the noise realizations is given by the channel impulse response (CIR) h_{kj} between the mesh network's power line outlets. Moreover, the CIR h_{kj} is directly related to the load impedance z_j.

- Temporal DN represents the deterministic relation between samples of the same noise time series at different time instances:

$$v^{(\mathrm{DN})}(t) = \mathcal{F}_{\mathrm{c}}[v(t-t_1), v(t-t_2), \dots]. \quad (6)$$

This effect is mainly caused by signal reflections produced by discontinuities of the PLN, and therefore, load mismatching. The noise signals arrive at the k-th power line outlet at different times, as a function of the discontinuities' topological position w.r.t. the k-th outlet.

- Spectral DN represents the deterministic relation between the noise signals at different frequency points:

$$V_k^{(\mathrm{DN})}(f) = \mathcal{F}_{\mathrm{d}}\big[V(f-f_1), V(f-f_2), \dots\big]. \quad (7)$$

This phenomenon is associated with impulsive noise and, thus, the wideband nature of noise signals. This type of noise is often generated by electric arcs, topological changes of the network, e.g., manual switches.

In the next two sections, we report two methodologies to identify and then model the MCO DN. We present a circuit-level and a phenomenological analysis.

III. CIRCUIT/NETWORK LEVEL ANALYSIS

The cause of deterministic phenomena can be investigated considering the relationships between the circuital components of the PLN. In this section, the linear relations between voltage, currents, and impedances are considered for this purpose. The objective is to understand if a specific configuration of the network and type of noise source produces a clear relation between the noise voltages measured at the ports of a specific power line outlet.

The relation between CTF and noise in PLC is not always straight forward. The noise reaches the PLC modems through conducted and radiated phenomena, resulting in multiple coupling effects. For example, cables mostly conduct the PLC signals but also radiate a certain percentage of them. Moreover, radio sources electromagnetic radiation in the surrounding environment is coupled to PLC modems through the air, or a mixture of air and cables, especially nearby discontinuities and interconnections [30]. The conducted effects of the PLN are well characterized since the PLN infrastructure is fixed, and therefore measurements are possible to characterize the medium. Differently, the radiation effects are in general difficult to model because depend on the objects and materials displaced in the surroundings of the cables. Therefore, characterization and modeling are much more challenging.

In this section, a general MIMO system (Fig. 1) is considered to analyze how the noise is coupled to the PLN. Then, the most common three-conductor system is analyzed in detail.

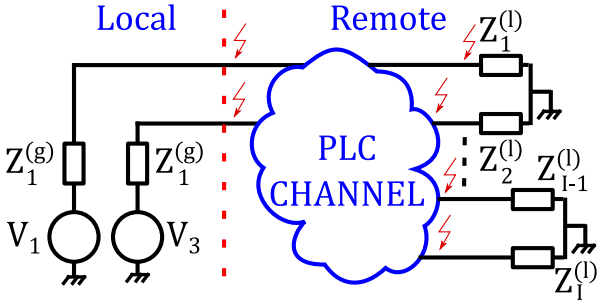

FIGURE 1. Equivalent model of a three-conductor power delivery network with possible noise sources.

The noise voltage in the frequency domain $V^{(L)}$, at a generic PLC outlet, also named as local (L) node, is modeled as the sum of radiated (r) and conducted (c) noise components coupled directly at the local node or coming from remote (R) paths, as follows

$$V^{(L)} = \sum_{j=1}^{J} V_j^{(r,L)} + \sum_{i=1}^{I} H_i V_i^{(c,R)} + \sum_{b=1}^{B} H_b V_b^{(r,R)}. \quad (8)$$

Where $V^{(r,L)}$ is the radiated noise coupled directly at the outlet. The radiated signal (r) is generated by the j-th noise source. $V^{(c,R)}$ is the remote noise conducted to the local node, and $V^{(r,R)}$ is the radiated component coming from a remote node of the PLN. The resulting noise at the local node is computed by multiplying the MCO CTFs (H_i, H_b) to the noises coupled at the remote nodes.

DETERMINISM FROM THE CIRCUITAL MODEL

The power line cable geometry substantially affects the CTFs. MCO flat cables have very different transmission characteristics w.r.t. round or separately shielded cables. Moreover, the geometry affects how the radiated signal is coupled to the network. This article aims to answer a fundamental question regarding the relations between CTFs and the DN component.

In a MCO, half-duplex PLC transmission system characterized by T independent sources and W receivers, the channel can be modeled with a matrix $\mathbf{H}$ of CTFs, with dimensions (W,T). Therefore, the noise is propagated from the sources to the receivers with the relation $V^{(L)} = \mathbf{H}V^{(R)}$. The signals received at the PLC modem ports are related to each other if the matrix is not full rank. As a result, the noise manifests a dependent relation among receiver ports due to dependency between the rows/columns of the matrix $\mathbf{H}$. This phenomenon happens, for example, when long power line MCO cables are shielded together using a symmetric geometry. Another cause can be the presence of filters or transformers in the channel branch.

$$\mathrm{rank}\big[\mathbf{H}_{(W,T)}\big] < \min(W,T) \text{ and } T \neq W, \quad (9)$$

$$V_{(w,k)}^{(L)} = \mathcal{F}\Big[V_{(w,j)}^{(L)}\Big], \text{ with } k \neq j, \text{ and } w \in W. \quad (10)$$

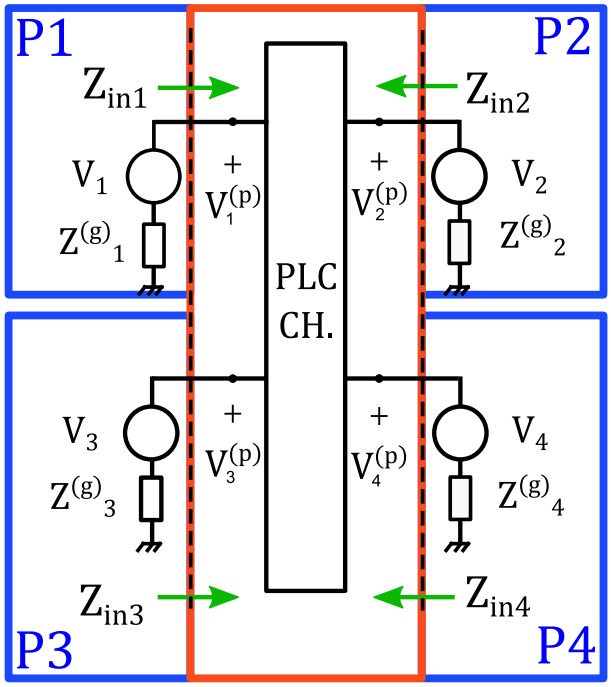

FIGURE 2. Schematic of ports in a three-conductor PLC system. The local node comprises two ports: P1 and P3; the remote node is connected to the local node by the PLC channel and comprises ports P2 and P4.

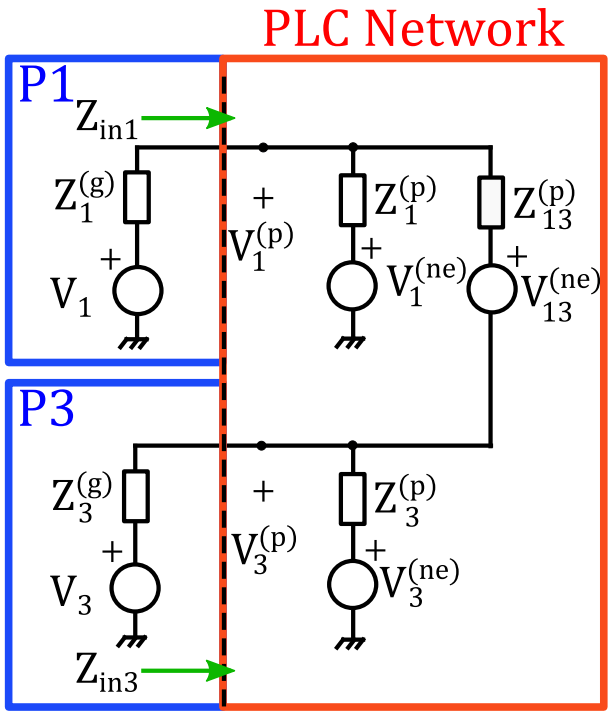

FIGURE 3. Equivalent PLC network representation seen from the two ports at the local node. The PLC network is represented by a π-network modeled with three load impedances and three voltage generators. The branch that includes Z^{p}_{13} and V^{ne}_{13} models the coupling effect between the two ports at the local node.

Therefore, the noise voltages at the local receiver w-th ($V^{(L)}_{(w)}$) are represented by a vector composed of $d = \max(W, T) - rank[\mathbf{H}_{(w,t)}]$, dependent parts, where the k-th one is written as a function of another j-th component.

A three-conductor and MIMO 2x2 system, graphically shown in Fig. 2, is considered to characterize the CTFs, impedances, and noise in detail. This model describes the relations between the noise at the local node (ports 1 and 3) and the remote node (ports 2 and 4).

In the schematic, the noise sources are modeled with voltage generators at the local (V_1, V_3) and remote (V_2, V_4) ports. The noise sources unify the following components: the noise generated inside the transceiver, the noise generated in the loads, the equivalent conducted noise, and the equivalent radiated noise sources. The PLN is modeled with a block (PLC CH.) that connects the four ports. The voltages at the local ports 1 and 3 are, for example, computed as follows:

$$\begin{aligned} V^{(p)}_1 &= H_{12}V^{(p)}_2 + H_{14}V^{(p)}_4, \\ V^{(p)}_3 &= H_{32}V^{(p)}_2 + H_{34}V^{(p)}_4. \end{aligned} \tag{11}$$

If we are only interested in the noise that arrives at the local node, the remote ports 2 and 4 represent the equivalent ports that summarize all the surrounding PLN.

The schematic in Fig. 2 can be further transformed to analyze the noise relation caused by the coupling between the two ports at the local node. For this purpose, it is convenient to transform the circuital model, as shown in Fig. 3. The conversion procedure is described in Appendix A. In this schematic, the PLC network effects are collapsed in three impedances $Z^{(p)}_1$, $Z^{(p)}_3$ and $Z^{(p)}_{13}$, while, the noise sources at the remote node are transformed to three equivalent generators $V^{(ne)}_1$, $V^{(ne)}_3$ and $V^{(ne)}_{13}$.

$$V^{(p)}_1 = V_1 - Z^{(g)}_1 I_1, \tag{12}$$
$$V^{(p)}_3 = V_3 - Z^{(g)}_3 I_3, \tag{13}$$
$$V^{(p)}_1 = Z^{(p)}_1 I^{(p)}_1 + V^{(ne)}_1, \tag{14}$$
$$V^{(p)}_3 = Z^{(p)}_3 I^{(p)}_3 + V^{(ne)}_3, \tag{15}$$
$$V^{(p)}_1 - Z^{(g)}_{13} I^{(p)}_{13} - V^{(ne)}_{13} = V^{(p)}_3. \tag{16}$$

The following equations consider these hypotheses: the impedances of the generators $Z^{(g)}_1$ and $Z^{(g)}_3$ are considered equal to $Z^{(g)}$; the radiated noise ($V^{(r)}$) is coupled in both ports with the same magnitude (valid if the radiative source is located sufficiently far from the PLC outlet). Solving the proposed circuit allows to describe the voltage at a particular PLC outlet and understand how the different noise components form the overall voltage signals. The noise components of $V^{(p)}_1$ and $V^{(p)}_3$ read:

$$\begin{aligned} V^{(p)}_1 &= V_1 + V^{(r)} + V^{(ss)} + V^{(os)} + V_{11}, \\ V^{(p)}_3 &= V_3 + V^{(r)} + V^{(ss)} - V^{(os)} + V_{33}. \end{aligned} \tag{17}$$

Analyzing the Eq.s (17), it's visible how some noise components of $V^{(p)}_1$ are also present in $V^{(p)}_3$. Some with the same sign ($V^{(ss)}$) other with opposite sign ($V^{(os)}$).

$$V^{(os)} = Z^{(g)}Z_1^{(p)}Z_3^{(p)}(V_3 + V_{13}^{(ne)} - V_1)/d,$$
$$V^{(ss)} = Z^{(g)2}\Big[V_1^{(ne)}Z_3^{(p)} + V_3^{(ne)}Z_1^{(p)} - V^{(r)}\Big(Z_1^{(p)} + Z_{13}^{(p)} + Z_3^{p}\Big)\Big]/d. \quad (18)$$

Where, the voltages V_{11}, V_{33} and the denominator d are computed as follows:

$$V_{11} = Z^{(g)}\Big[Z^{(g)}\Big(V_1^{(ne)}Z_{13}^{(p)} + V_{13}^{(ne)}Z_1^{(p)} - V_1\Big(Z_{13}^{(p)}Z_1^{(p)} + Z_3^{(p)}\Big)\Big) + Z_{13}^{(p)}Z_3^{(p)}\Big(V_1^{(ne)} - V_1 - V^{(r)}\Big)\Big]/d, \quad (19)$$

$$V_{33} = -Z^{(g)}\Big[Z^{(g)}\Big(V_3^{(ne)}Z_{13}^{(p)} - V_{13}^{(ne)}Z_3^{(p)} - V_3\Big(Z_3^{(p)} + Z_{13}^{(p)}Z_1^{(p)}\Big)\Big) + \Big(Z_{13}^{(p)}Z_1^{(p)}\Big(V_{13}^{(ne)} - V_3 - V^{(r)}\Big)\Big]/d, \quad (20)$$

$$d = 2Z^{(g)}Z_1^{(p)}Z_3^{(p)} + Z_{13}^{(p)}Z^{(g)}Z_3^{(p)} + Z_{13}^{(p)}Z^{(g)}Z_1^{(p)} + Z_{13}^{(p)}Z_1^{(p)}Z_3^{(p)} + Z^{(g)2}\Big(Z_1^{(p)} + Z_3^{(p)} + Z_{13}^{(p)}\Big). \quad (21)$$

Supposing that the noise generated inside the transceiver has low power w.r.t. the noise coming from the PLN (true if the PLC transceiver is properly designed); then, $(V_1, V_3) << (V^{(r)}, V_1^{(ne)}, V_3^{(ne)}, V_{13}^{(ne)})$. Therefore, the equations can be simplified considering negligible the effect of V_1 and V_3.

$$V_1^{(p)} \approx V^{(r)} + V^{(ss)} + V^{(os)} + V_{11}, \quad (22)$$
$$V_3^{(p)} \approx V^{(r)} + V^{(ss)} - V^{(os)} + V_{33}, \quad (23)$$
$$V^{(os)} \approx Z^{(g)}Z_1^{(p)}Z_3^{(p)}V_{13}^{(ne)}/d, \quad (24)$$
$$V^{(ss)} = \text{ not changed.} \quad (25)$$

The voltages V_{11} and V_{33} are rewritten as

$$V_{11} \approx Z^{(g)}\Big[Z^{(g)}\Big(V_1^{(ne)}Z_{13}^{(p)} + V_{13}^{(ne)}Z_1^{(p)}\Big) + Z_{13}^{(p)}Z_3^{(p)}\Big(V_1^{(ne)} - V^{(r)}\Big)\Big]/d, \quad (26)$$

$$V_{33} \approx -Z^{(g)}\Big[Z^{(g)}\Big(V_3^{(ne)}Z_{13}^{(p)} - V_{13}^{(ne)}Z_3^{(p)}\Big) + Z_{13}^{(p)}Z_1^{(p)}\Big(V_{13}^{(ne)} - V^{(r)}\Big)\Big]/d. \quad (27)$$

In the case of dependent channels, the further hypothesis of having $Z_1^{(p)}$ and $Z_3^{(p)}$ equal to an impedance $Z^{(p)}$, leads to

$$V^{(os)} \approx Z^{(g)}\Big(Z^{(p)}\Big)^2 V_{13}^{(ne)}/d,$$
$$V^{(ss)} = Z^{2(g)}\Big[Z^{(p)}\Big(V_1^{(ne)} + V_3^{(ne)}\Big) - V^{(r)}\Big(2Z^{(p)} + Z_{13}^{(p)}\Big)\Big]/d. \quad (28)$$

Furthermore, in the case of high common noise injected at the remote node, the noise voltage $V_{13}^{(ne)}$ is negligible. Then, the noise at the local node at both ports is characterized only by the signal $(V^{(ss)})$.

$$V^{(os)} \approx 0,$$
$$V^{(ss)} = Z^{2(g)}\Big[Z^{(p)}2V^{(ne)} - V^{(r)}\Big(2Z^{(p)} + Z_{13}^{(p)}\Big)\Big]/d. \quad (29)$$

The obtained equations support the thesis that high radiated signal at the local or remote node leads to DN at the receiver.

In this section, the relations are expressed as functions of voltages and impedances. These relations can be used to compute the Power Spectral Density (PSD) as follows:

$$P^{\mathrm{vv}}(f) = \lim_{T\to\infty}\frac{\mathbb{E}\big[|V^T(f)|^2\big]}{T}, \quad (30)$$

where, V_T is the Fourier transform of the voltage signal $v(t)$ in a finite time interval of length T, and $\mathbb{E}$ denotes the statistical expectation.

IV. PHENOMENOLOGICAL ANALYSIS

The PLC DN component is often not negligible and sometimes also greater than the SN one. In this section, three available metrics are proposed to identify the deterministic component characteristics: the cross-correlation, the distance correlation, and the estimated mutual information. Moreover, we also define the linear coefficient ratio between MCO voltage noise traces. Then, these metrics will be used in Section VI to process the measured data and derive a model. In the next paragraphs, formulas will be illustrated for the two-ports case.

The considered signals represent the noise at the local ports P1 and P3 acquired at the same PLC outlet. They are modeled with two discrete time random processes, $v_1^k(n)$ and $v_3^k(n)$, defined in a time window k of L samples and duration T, where n denotes the sample index. The processes are considered, by hypothesis, stationary in the window time-interval.

A. THE CROSS-CORRELATION METHOD

The cross-correlation $r^k(m)$ is defined between the two noise voltage signals in discrete time as follows

$$r^k(m) \equiv \mathbb{E}\Big[v_1^k(n+m)v_3^k(n)\Big], \quad (31)$$

where m represents the shift in samples between the two signals. The method, as mentioned above, measures the linear relation between the two noise voltage signals. However, non-linear relationships are not considered. Therefore, the correlation method gives only a first indication of the two variables' relation and may not be enough to measure all noise dependencies.

B. THE DISTANCE CORRELATION METHOD

A more precise metric to test the relation of noise signals is the distance correlation. The distance correlation has been introduced in [33] and provides an approach to the problem of testing the joint independence of random signals. For all distributions with finite first moments, distance correlation d_r generalizes the idea of correlation. The distance correlation has properties of a true dependence measure, analogous

to the product-moment correlation r. Moreover, it satisfies $0 \leq d_r \leq 1$. The correlation d_r is defined, between two variables x and y, that for the scope of this article, represent the noise voltages $v_1^k(n)$ and $v_3^k(n)$. In [33] the distance correlation is explained in detail. The distance correlation has the interesting property of being zero only when the noise time series are independent. Therefore, it is more informative than the cross-correlation method.

C. THE MUTUAL INFORMATION METHOD

Among the metrics to verify dependence between time series, Mutual Information (MI) has an important role [34]. In contrast to the cross-correlation coefficient, it is sensitive to dependencies that do not manifest themselves in the covariance. The MI can be interpreted as a generalized measure of correlation, analogous to Pearson correlation, but sensitive to any functional relationship, not just linear dependencies [35].

Exploiting the Kullback definition, the mutual information is considered a measure of the distance between probability distributions. For the purpose of this article, we are interested in the estimation the MI of two noise voltage signals $v_1^k(n)$ and $v_3^k(n)$ as follows:

$$\mathrm{MI}^k = \mathbb{E}\left[\log \frac{p_{(v_1^k, v_3^k)}}{p_{(v_1^k)} p_{(v_3^k)}}\right], \tag{32}$$

MI^k is equal to zero only if the probability distribution of $v_1^k(n)$ and $v_3^k(n)$ are identical. In general, probability distributions are unknown and have to be estimated from measurement data. Multiple strategies are possible to achieve this goal. In this article, the estimation technique proposed in [34] is used to estimate the MI^k for noise voltage time series divided in windows k of L samples.

D. THE LINEAR COEFFICIENT RATIO

The Linear Coefficient Ratio (LCR) is herein proposed to characterize the linear dependencies between noise signals and precisely quantify the MCO DN. For a three conductor system the noise model defined in Eq. (2) translates into its MCO discretized version

$$\begin{aligned} v_1^k(n) &= v_1^{(\mathrm{DN}),k}(n) + v_1^{(\mathrm{SN}),k}(n), \\ v_3^k(n) &= v_3^{(\mathrm{DN}),k}(n) + v_3^{(\mathrm{SN}),k}(n). \end{aligned} \tag{33}$$

The deterministic effect is measurable when the deterministic components have a higher magnitude w.r.t. the SN ones. Therefore, it is possible to introduce a parameter $\alpha^k(m)$ defined as the expectation of the ratio of the measured noise at the local ports, for a given window k of duration T, as shown in Eq. (34), to provide an immediate understanding of the phenomena. Specifically, the estimation of $\alpha(m)$ leads to a metric that allows to evaluate if the SN component is negligible w.r.t. the deterministic one.

$$\begin{aligned} \alpha^k(m) &= \mathbb{E}\left[\frac{v_3^k(n+m)}{v_1^k(n)}\right], \\ &\approx \mathbb{E}\left[\frac{v_3^{(\mathrm{DN}),k}(n+m)}{v_1^{(\mathrm{DN}),k}(n)}\right], \end{aligned} \tag{34}$$

where, m is the shift in samples between the noise at the ports 1 and 3, and k is the time window index under analysis. Applying on Eq. (34) a moving average on K subsequent windows, we obtain

$$\overline{\alpha}^k(m) = \frac{\sum_{j=0}^{K-1} \alpha^{k-j}(m)}{K}. \tag{35}$$

Similarly, in the frequency domain, we can define the parameter $\beta(f)$ as the ratio between two spectral representations of noise signals as follows

$$\beta^k(f) = \frac{V_3^k(f)}{V_1^k(f)} \approx \frac{V_3^{(\mathrm{DN}),k}(f)}{V_1^{(\mathrm{DN}),k}(f)}, \tag{36}$$

where f is the frequency index. Applying on Eq. (36) a moving average on K subsequent windows we obtain

$$\overline{\beta}^k(f) = \frac{\sum_{j=0}^{K-1} \beta^{k-j}(m)}{K}. \tag{37}$$

The estimation of the parameter $\overline{\alpha}^k(0)$ will be used to evaluate if the SN component is negligible w.r.t. the deterministic one. Moreover, the parameter $\overline{\beta}^k(f)$ will be used to derive noise mitigation algorithms in Section VII.

V. EXPERIMENTAL EVIDENCE

In this section, the theoretical considerations previously presented are verified using real noise data. The data is collected mainly in the laboratories and offices of the University of Klagenfurt (Austria) in more than 100 different outlets. The noise signal is acquired concurrently from both ports of the three-conductor network in the PLC broadband spectrum (1-50MHz). Specifically, noise traces are sampled at 100Ms/s, have duration 20ms, and are acquired several times at each considered outlet port. In addition, 2x2 MIMO CTFs and line impedance matrices are measured at the same nodes where the noise is acquired. The dataset of measured channels, impedances, and noise traces is described in Appendix B.

A. COMPARISON OF METHODS TO DETECT DETERMINISM

The metrics presented in Section IV are compared to understand which one is the most effective to characterize the DN. The noise dataset of two-port outlets is grouped in smaller windows of L samples (with sampling period 10ns). Then, the metrics are computed for each window k. The realizations are visualized in Figs. 4 and 5. In Fig. 4, the Mutual Information (MI) is graphed as a function of the cross-correlation coefficient $r^k(0)$, with lag $m = 0$.

Fig. 5, shows how the distance correlation (d_r) and the cross-correlation metrics are related. The graph shows almost a linear relation with long windows. While, for a small L, the graph highlights the benefits of the distance correlation in

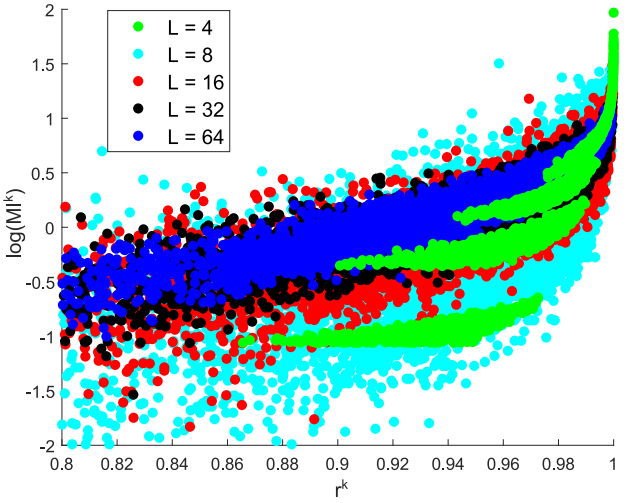

FIGURE 4. The logarithm of the MI^k as a function of the cross-correlation $r^k(0)$, for all noise windows k, each comprising L samples.

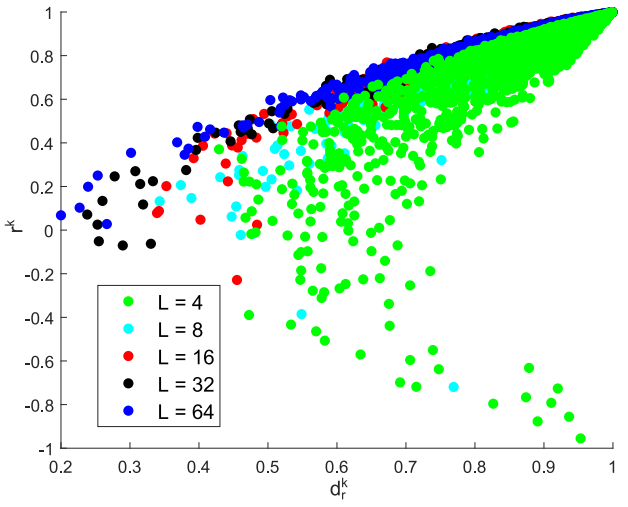

FIGURE 5. The cross-correlation $r^k(0)$, as a function of the distance correlation d_r^k, for all noise windows k, each comprising L samples.

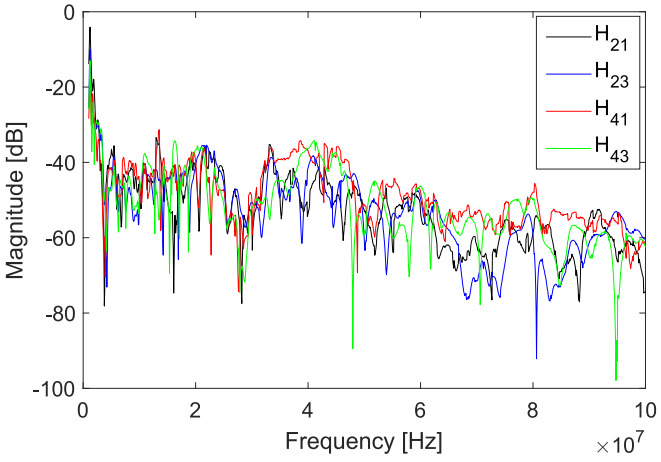

FIGURE 6. Example of PLC channel frequency response measurement. The PLC channel has been acquired in the BB spectrum (1-100MHz) with a Vector Network Analyzer (VNA) synchronized to the mains period. The magnitudes of the four CTFs are for several frequency point very similar, especially for low frequencies.

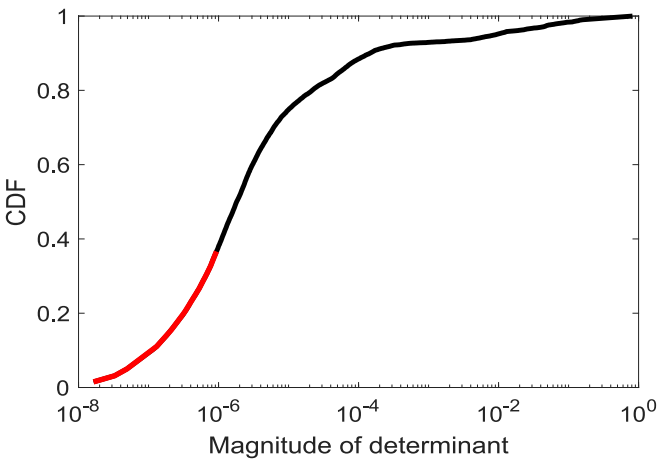

FIGURE 7. Estimated CDF of the magnitude of the MIMO channel matrix determinant computed with the dataset of real channel measurements. The CDF shows a probability of about 0.35 to obtain determinant values less than 10^{-6}.

identifying the determinism. Unlike the cross-correlation that spans all range between -1 and 1, the distance correlation has values only above 0.4. This result proves that short noise windows are always partially related and never independent across MCOs.

In general, the PLC noise shows the classical U shape (also obtained with Gaussian noise [36]) of the cross-correlation as a function of the MI. Moreover, the noise patterns are visibly separated if the time window length (L) is decreased. Thus, groups of different noise types are visible. This is clear observing Fig. 4 with $L = 4$, and suggests also a temporal-determinism between samples.

B. CHANNEL AND INPUT IMPEDANCE CHARACTERISTICS THAT INFLUENCE THE NOISE DEPENDENCY

In Section III, it has been shown that the network topology and symmetric MCO displacement is one of the reasons for the presence of the noise determinism among the MCOs. In more detail, this is expected to be the case when the matrix H that collects the CTFs is rank deficient. Graphically, this phenomenon is visible when the magnitude of the CTFs is very similar. Fig. 6 shows an example of a specific CTFs realization, where H_{12}, H_{32}, H_{14} and H_{34} are very similar for several frequency points in the range 1 - 100MHz. Here, H_{ij} considers the local ports (i = 1, 3) as receiving ports, as represented in Eq. (11).

A method to analyze the rank of the matrix $\mathbf{H}$ is through the evaluation of its determinant (det(H)). If the determinant approaches zero, we can claim the channel to be rank deficient. Fig. 7 shows the determinant magnitude Cumulative Distribution Function (CDF). For a considerable percentage (about 35% of the channel realizations in the dataset) of CTF realizations, the determinant is below 10^{-6}, thus, causing MIMO matrix rank deficiencies.

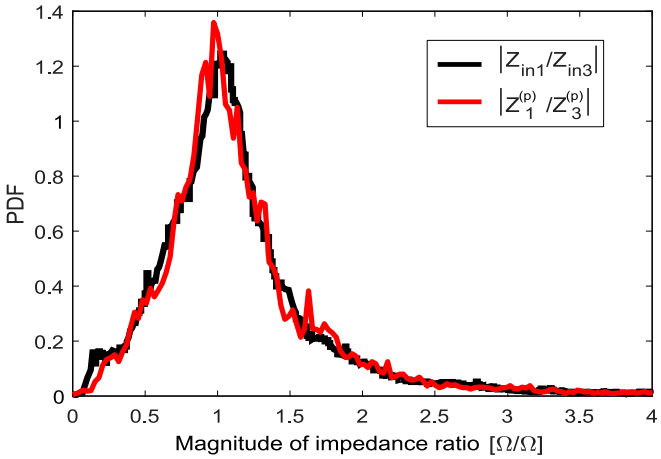

FIGURE 8. Estimated PDF of the input impedance ratio magnitude extracted by measurements (black curve). Estimated PDF of the ratio $Z_1^{(p)}$ and $Z_3^{(p)}$ used in Fig. 3 and explained in Appendix A (red curve). The results show that with high probability, such a ratio takes value one.

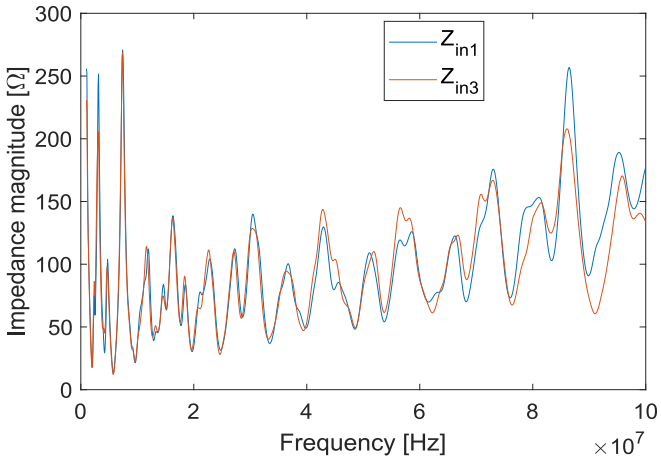

FIGURE 9. Example of measured PLC input impedances magnitude. The PLC input impedances have been acquired in the BB spectrum (1-100MHz) with a Vector Network Analyzer (VNA) synchronized to the mains period.

Another important parameter derived from the measurement campaigns is the input impedance. The input impedance values are used to understand how the signal is flowing from the transmitter to the network and between the MCOs. In Section III, it has been mentioned that a symmetry in the port impedances $Z_1^{(p)}$ and $Z_3^{(p)}$, together with high common mode noise, leads to DN at the ports 1 and 3. These equivalent impedances are directly related to the port input impedances Z_{in1} and Z_{in3} as explained in Eq. (58). An example of input impedances realization is shown in Fig. 9. In this figure, it is visible that the impedance magnitude of the two ports at the local node is practically the same for several frequency intervals. Consequently, the signal and noise injected at the local ports are evenly divided into the two MCO channels. Therefore, the impedance similarity contributes to the generation of DN components. Numerically, this characteristic has been analyzed computing the PDF of the magnitude of the input impedance ratio: $|Z_{in1}/Z_{in3}|$ for

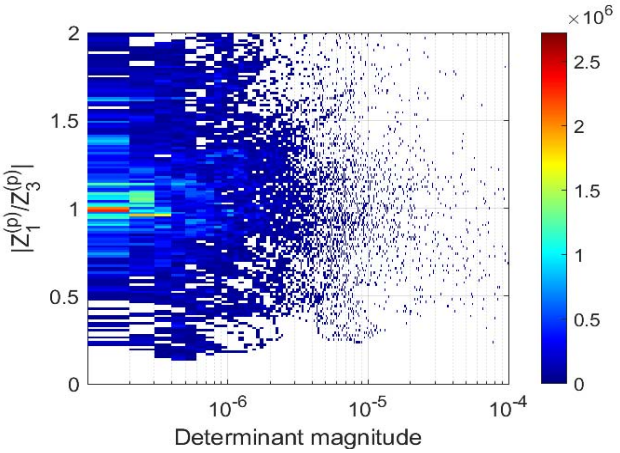

FIGURE 10. Estimated bivariate PDF of the MIMO channel matrix determinant magnitude and the impedance ratio $|Z_1^{(p)}/Z_3^{(p)}|$.

all measurements in the dataset. Fig. 8 shows that the PDF of the ratio is a curve centered in one. Thus, it confirms that, on average, the impedance realizations at the local node ports are very similar.

Moreover, to highlight the relation between dependent channels and similarity of $Z_1^{(p)}$ and $Z_3^{(p)}$, the estimated bivariate PDF of the determinant magnitude of the matrix H and the ratio $|Z_1^{(p)}/Z_3^{(p)}|$ is shown in Fig. 10. The color bar represents the magnitude of the estimated bivariate PDF. We found that it is highly probable that the ratio $|Z_1^{(p)}/Z_3^{(p)}|$ is one for very low determinant magnitudes. About 30% of the channel realizations in the dataset are in the range: $0.8 < |Z_1^{(p)}/Z_3^{(p)}| < 1.2$ and $\det(H) < 10^{-6}$.

It has to be remarked that the MIMO channels dependency is only one of the possible causes of multi-conductor noise determinism. Other situations that lead to deterministic noise components cannot be analyzed considering only the MIMO CTFs and input impedance values. An example is the radiated noise coupled directly at the two receiver ports. This noise might also show a deterministic behavior that is not imputable to the MIMO CTFs characteristics of the PLC network. Therefore, a phenomenological analysis of measured noise traces is done in the next section.

C. MULTI-CONDUCTOR NOISE ANALYSIS

In this section, direct analysis of the noise trends is performed using the dataset described in Appendix B. The noise traces are analyzed in both time and frequency domain considering consecutive time slots k.

Fig. 11 shows an example of LCR estimated according to Eq. 35, for a PLC noise trace, acquired at a specific outlet. The figure left-side shows the PDFs, and the right-side shows the trends in time of $\overline{\alpha}^k(0)$ for different windows k of length $L = (4, 64, 256, 1024)$. For short windows of $L = 4$, aperiodic and periodic patterns with a period of approximately 4us are visible. For $L = 64$ abrupt changes of $\overline{\alpha}^k(0)$ are visible with intervals between 20 and 30us. With longer

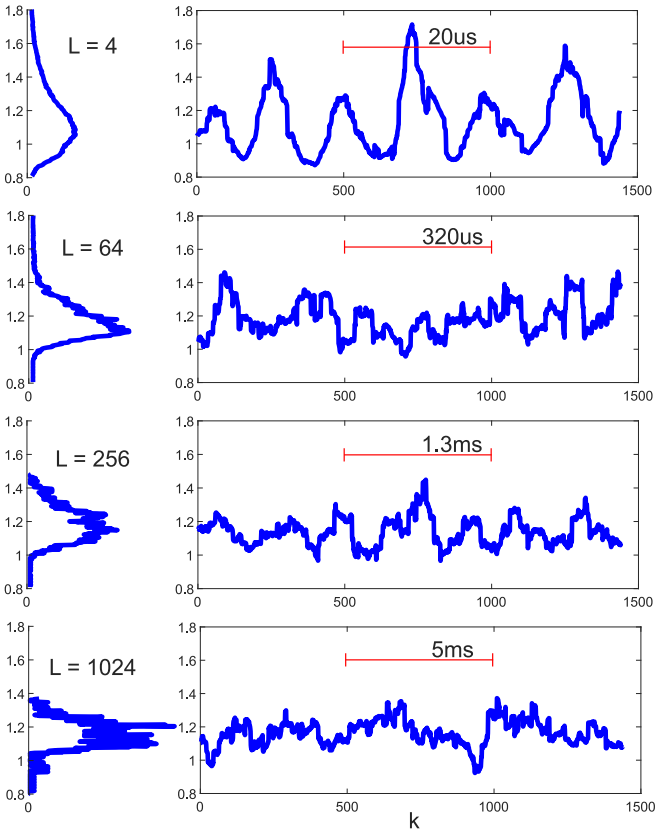

FIGURE 11. Parameter $\overline{\alpha}^k(0)$, for windows of length: $L = (4, 64, 256, 1024)$ samples. On the left-side the estimated PDFs and on the right the parameter $\overline{\alpha}^k(0)$ as a function of the window index k. Considering a moving average of $K = 60$ windows.

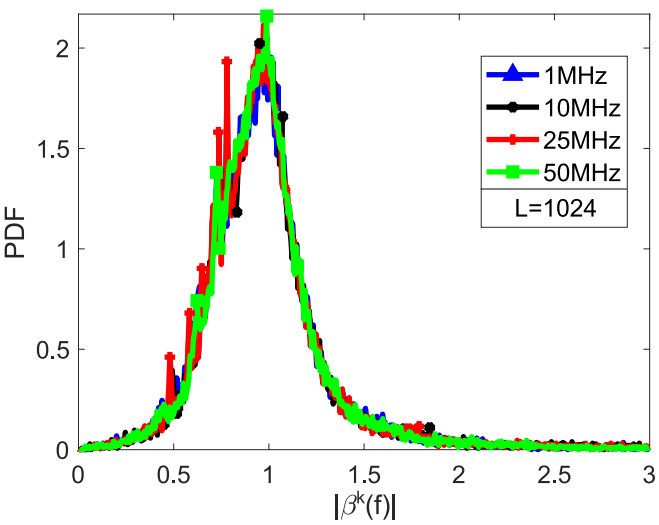

FIGURE 12. Estimated PDF of the magnitude of the parameter $\beta^k(f)$, for windows of $L = 1024$ and frequencies $f = (1, 10, 25, 50)$ MHz. All available noise traces in the dataset are used to compute $\beta^k(f)$.

windows, the patterns are more chaotic, and the variance w.r.t the mean is lower. With windows of length $L = 1024$, (e.g., used exploiting OFDM transmission systems), $\overline{\alpha}^k(0)$ is confined around 1.2, with standard deviation of approximately 0.3. However, on a short period of $K \approx 100$ subsequent windows, the variance is often minimal and thus, $\overline{\alpha}^k(0)$ can be approximated as static.

Fig. 12 shows the magnitude of $\overline{\beta}(f)$, i.e., estimated according to Eq. (36) considering all noise traces in the dataset and a window length $L = 1024$. The PDF of $\overline{\beta}(f)$ is computed separately for the frequencies: 1, 10, 25 and 50MHz. All curves show a bell shape centered in the region where $\overline{\beta}(f)$ is approximately one. It is possible to notice that for frequencies equal to 25 and 50MHz, the bell shape is noisier and presents peaks at several values between 0.5 and 1. These peaks in the PDF highlight that for several noise traces in the dataset $\overline{\beta}(f)$ assumes values around these peaks with an high probability. The computation of the LCRs have been obtained considering $|\alpha^k(0)| < 10$ and $|\beta^k(f)| < 10$ to avoid numerical errors.

In most noise windows, the LCRs assume values in the range of 0.5 and 1.5. However, considering specific PLC outlets and short periods, the LCRs standard deviation is significantly reduced, and in some cases, LCR can be considered constant. This evidence allows us to estimate the LCR and exploit it to predict the relation between noise traces acquired at adjacent power line conductors.

VI. QUASI DETERMINISTIC NOISE MODEL

In the previous section, experimental metrics have been computed from real noise traces to extract information that identifies the presence of determinism. Another aspect not yet addressed is identifying a situation where determinism occurs, i.e., classify whether we are in the presence of determinism.

Now, inferring a linear relation between the DN components on the port 1 and 3, of a given node, and exploiting the definition of the coefficient $\overline{\alpha}^k(0)$, Eq. (33) can be written in the discrete form as follows:

$$\begin{aligned} v_1^k(n) &= v_1^{(\mathrm{DN}),k}(n) + v_1^{(\mathrm{SN}),k}(n), \\ v_3^k(n) &= \overline{\alpha}^k(0) v_1^{(\mathrm{DN}),k}(n) + v_3^{(\mathrm{SN}),k}(n). \end{aligned} \tag{38}$$

An important question is related to determining the condition for the model validity. In other words, define when the DN component is larger than the SN one, and therefore, the proposed model in Eq. (38) is valid. For this purpose we define the probability

$$P_{\overline{\alpha}^k(0)} = P\Big[\Big(\overline{\alpha}^k(0) - \epsilon\Big) \le \overline{\alpha}^k(0) \le \Big(\overline{\alpha}^k(0) + \epsilon\Big)\Big] > P^{(\mathrm{DN})}. \tag{39}$$

When $P_{\overline{\alpha}^k(0)}$ is greater than a threshold value $P^{(\mathrm{DN})}$ we assume that the noise is mainly deterministic. Specifically, $P^{(\mathrm{DN})}$ is a threshold value for which we can assume the noise QD, and 2ϵ is the interval for which $\overline{\alpha}^k(0)$ is likely to be estimated.

Theoretically, a sample is considered deterministic if the MI tends to infinity. However, because of numerical problems and the presence of SN, the MI estimation technique

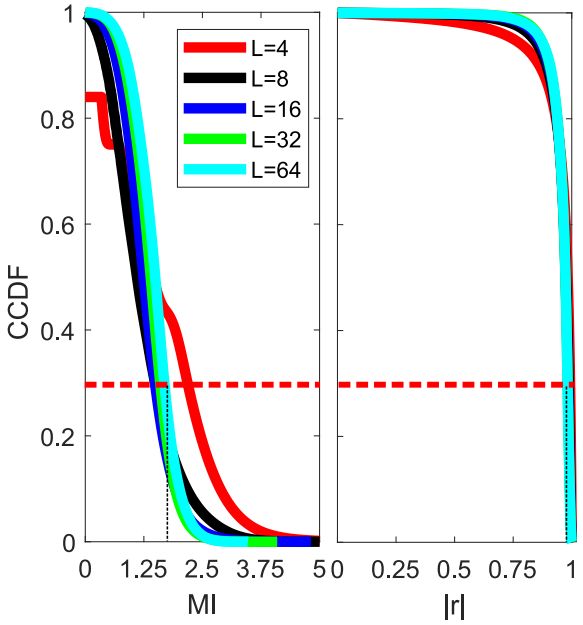

FIGURE 13. Estimated CCDF of MI and $|r|$ for noise windows of multiple lengths.

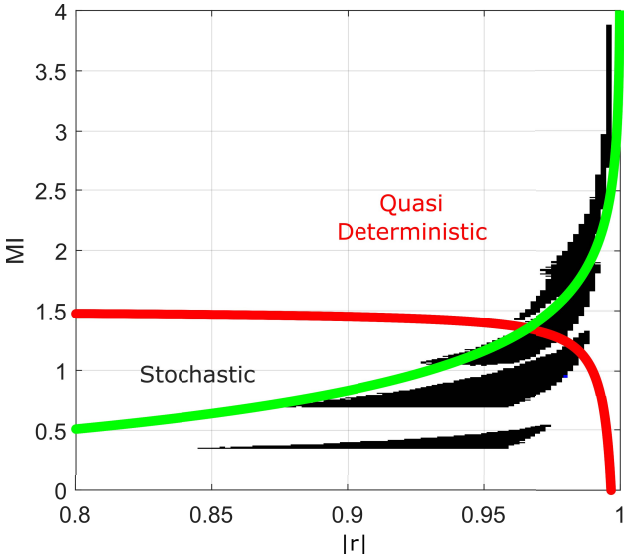

FIGURE 14. Estimated MI as a function of the cross-correlation for the case of noise windows of four samples. The red hyperbola represent the limit to assume deterministic a noise window. The green line is used as reference and represents the result obtained with Gaussian noise realizations.

leads to finite values. Therefore, we can define a heuristic region where the noise realizations assume deterministic behaviors, that we can refer to as QD.

The CCDF respectively of the MI and $|r|$ realizations, have been used as metric to identify $P^{(\mathrm{DN})}$. Fig. 13, shows these parameters for several noise windows lengths (L = 4, 8, 16, 32, 64). The determinism region is identified in correspondence to the highest values of MI and correlation. Therefore, heuristically, after experimentations a threshold value at $P^{(\mathrm{DN})} = 0.3$ and $2\epsilon = 0.1$ were defined as separation parameters to categorize the SN and QD noise realizations. Thus, the QD region is described with $P[\mathrm{MI} > 1.32 \cap |r| > 0.98] = 0.3$.

The same conclusion is obtained from a different perspective exploiting the relation between MI and correlation coefficient, as graphically displayed in Fig. 14. The hyperbola (displayed in red) cuts the plane into two regions. The noise realizations that lay above the hyperbola are considered deterministic. In contrast, the realizations below the red line are considered stochastic. The hyperbola is defined based on Eq. (39) as follows

$$(|r| - 1)(\mathrm{MI} - 1.5) = 0.005. \tag{40}$$

The green line represents the reference trend obtained by considering the relation between MI and $|r|$ computed from Gaussian noise.

VII. IMPLICATIONS AT THE RECEIVER

In the previous sections, we have shown that noise is, in many instances, predominantly deterministic across MCOs. Therefore, a natural question arises: *is it possible to remove it at the receiver side?* This section proposes some simple SIMO and MIMO transmission configurations and coding schemes that exploit decoding algorithms that take advantage of the noise determinism to offer improved performance. The algorithms aim to mitigate noise at the receiver by removing the MCO ports' deterministic component. The decoding techniques that exploit the proposed noise model are called QD-Decoding. The 1x2 SIMO and 2x2 MIMO systems have been simulated using measured channel responses and noise traces. Data bits are firstly mapped into binary-phase-shift-keying (BPSK) or 4PSK data symbols and then modulated using OFDM in the PLC BB spectrum (1-50MHz). To offer practical evidence that performance can be improved by deploying MCO signal processing, both SIMO and MIMO configurations are considered. It should be noted that both SISO and MIMO PLC standards and commercial products for in-home applications exist. The proposed algorithms that exploit the noise determinism knowledge are compared to conventional decoding schemes, such as maximum-likelihood detection (ML). In Section VII-D the performance is evaluated in terms of bit-error-rate (BER). For the SIMO case, the classic ML method (abbreviated with SIMO-ML) is compared with the SIMO-QD method that exploits the deterministic model. Moreover, the MIMO-QD-E algorithm has an overall coding rate of 1 with two simultaneous signal transmissions. Therefore, we compare it with the SIMO uncoded methods at equal rate. For the MIMO case, the classical decoding schemes that exploit ML (MIMO-ML) and linear decoding (MIMO-L) are compared with two new algorithms that exploit the QD model: MIMO-QD-D and MIMO-QD-L."

A. DECODING TECHNIQUES FOR SIMO COMMUNICATION

Assuming SIMO transmission without any coding, the received signals Y_1 and Y_3 in the frequency domain,

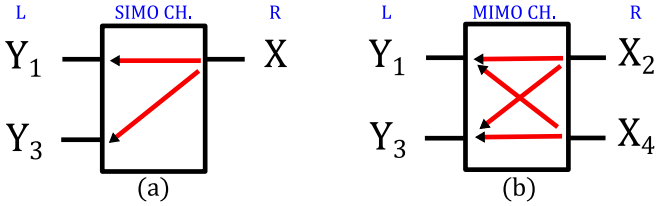

FIGURE 15. Schematics of SIMO 1x2 and MIMO 2x2. Arrows indicate the signals' directions: from the remote (R) node to the local (L) one.

exploiting the schematic in Fig. 15(a), can be modeled as follows:

$$Y_1 = XH_{12} + N_1^{(\mathrm{DN})} + N_1^{(\mathrm{SN})},$$
$$Y_3 = XH_{32} + \beta N_1^{(\mathrm{DN})} + N_3^{(\mathrm{SN})}, \tag{41}$$

where, X represents the transmitted data symbol, $N_1^{(\mathrm{DN})}$ is the QD noise component, $N_1^{(\mathrm{SN})}$ and $N_3^{(\mathrm{SN})}$ are the SN components respectively at the receiver 1 and 3. The parameter β, estimated with the LCR method proposed in Section IV-D is used to represent the QD noise effect between ports 1 and 3. While, H_{12} and H_{32} are the SIMO CTFs from the remote port 2 to the local ports 1 and 3.

It should be noted that β is frequency dependent, however it can be considered constant over the transmission time of several OFDM symbols.

Before the decoding procedure, the parameter β and the channel transfer functions (H_{12} and H_{32}) are estimated through a training procedure, as detailed in Section VII-C. The DN component is estimated for each received symbol during the ML procedure, subtracting from Y_1 the effect of the channel ($X\hat{H}_{12}$). The SN components can be considered negligible w.r.t. the deterministic ones. The SIMO-QD decoding algorithm has the following ML cost function:

$$\hat{X}^{\mathrm{QD}} = \mathrm{argmin}_{\tilde{X}}\left\{\left|Y_3 - \tilde{X}\hat{H}_{32} - \hat{\beta}Y_1 + \hat{\beta}\tilde{X}\hat{H}_{12}\right|^2\right\}, \tag{42}$$

where $\hat{X}^{\mathrm{QD}}$ is the estimated data symbol exploiting the SIMO-QD approach.

Differently, if the noise determinism is not exploited (i.e., Eq. (41) with the DN components equal to zero), a conventional ML algorithm called SIMO-ML can be used:

$$\hat{X}^{\mathrm{ML}} = \mathrm{argmin}_{\tilde{X}}\left\{\left|Y_3 - \tilde{X}\hat{H}_{32}\right|^2 + \left|Y_1 - \tilde{X}\hat{H}_{12}\right|^2\right\}, \tag{43}$$

where $\hat{X}^{\mathrm{ML}}$ is the estimated symbol with the classical SIMO-ML algorithm.

B. DECODING TECHNIQUES FOR MIMO COMMUNICATION

The received signals Y_1 and Y_3, in the case of a MIMO 2x2 transmission system can be modeled in the frequency domain, exploiting the schematic in Fig. 15(b), as follows:

$$Y_1 = X_2H_{12} + X_4H_{14} + N_1^{(\mathrm{DN})} + N_1^{(\mathrm{SN})},$$
$$Y_3 = X_2H_{32} + X_4H_{34} + \beta N_1^{(\mathrm{DN})} + N_3^{(\mathrm{SN})}, \tag{44}$$

where, X_2 and X_4 are the symbols sent respectively from ports 2 and 4. $N_1^{(\mathrm{DN})}$ is the QD noise component, $N_1^{(\mathrm{SN})}$ and $N_3^{(\mathrm{SN})}$ are the SN components respectively at the receiver 1 and 3. The MIMO CTFs are H_{12}, H_{14}, H_{32} and H_{34}. The parameter β, computed with the LCR method is used to represent the QD noise effect between ports 1 and 3.

In the MIMO case, we can firstly consider two baseline decoding schemes, i.e., a linear (MIMO-L) and a ML decoder (MIMO-ML). In the former case, the received voltage vector is multiplied by the inverse channel matrix. In the latter case, the ML metric reads as follows:

$$\left[\hat{X}_2, \hat{X}_4\right]^{\mathrm{ML}} = \mathrm{argmin}_{\tilde{X}_2,\tilde{X}_4}\left\{\left|Y_1 - \tilde{X}_2\hat{H}_{12} - \tilde{X}_4\hat{H}_{14}\right|^2 + \right.$$
$$\left. + \left|Y_3 - \tilde{X}_2\hat{H}_{32} - \tilde{X}_4\hat{H}_{34}\right|^2\right\}, \tag{45}$$

where, $[\hat{X}_2, \hat{X}_4]^{\mathrm{ML}}$ are the estimated symbols with the MIMO-ML algorithm. Both baseline decoders do not consider QD noise components. Therefore, β and $\hat{N}^{(\mathrm{DN})}$ are considered equal to zero.

Considering the QD model, three decoding schemes are herein proposed. The MIMO Quasi Deterministic Decoupling (MIMO-QD-D) method uncouples the Eq.s (44) subtracting from the received signals the effect of the DN ($\hat{N}^{(\mathrm{DN})}$). The DN is estimated continuously in time and for each symbol as follows

$$\hat{N}^{(\mathrm{DN})} = 0.5\Big(Y_1 - \tilde{X}_2\hat{H}_{12} - \tilde{X}_4\hat{H}_{14} + $$
$$+ \left(Y_3 - \tilde{X}_2\hat{H}_{32} - \tilde{X}_4\hat{H}_{34}\right)/\hat{\beta}\Big). \tag{46}$$

The MIMO-QD-D method exploits the following ML cost function:

$$\left[\hat{X}_2, \hat{X}_4\right]^{\mathrm{QD\text{-}D}} = \mathrm{argmin}_{\tilde{X}_2,\tilde{X}_4}\left\{\left|Y_1 - \tilde{X}_2\hat{H}_{12} - \tilde{X}_4\hat{H}_{14} + \right.\right.$$
$$\left. - \hat{N}^{(\mathrm{DN})}\right|^2 + \left|Y_3 - \tilde{X}_2\hat{H}_{32} - \tilde{X}_4\hat{H}_{34}\right.$$
$$\left.\left. - \hat{\beta}\hat{N}^{(\mathrm{DN})}\right|^2\right\}. \tag{47}$$

A variation of the MIMO-QD-D method called MIMO Quasi Deterministic Linear (MIMO-QD-L), exploits the sum ($Z = Y_1 + Y_3$) and subtraction ($R = Y_1 - Y_3$) of the received signals Y_1 and Y_3. Its ML cost function reads as follows:

$$\left[\hat{X}_2, \hat{X}_4\right]^{\mathrm{QD\text{-}L}} = \mathrm{argmin}_{\tilde{X}_2,\tilde{X}_4}\left\{\left|Z - \left[\tilde{X}_2\left(\hat{H}_{12} + \hat{H}_{32}\right) + \right.\right.\right.$$
$$\left. + \tilde{X}_4(\hat{H}_{14} + \hat{H}_{34}) + \hat{N}^{(\mathrm{DN})}(1 + \hat{\beta})\right]\Big|^2 +$$
$$+ \left|R - \left[\tilde{X}_2\left(\hat{H}_{12} - \hat{H}_{32}\right) + \right.\right.$$
$$\left.\left.\left. + \tilde{X}_4\left(\hat{H}_{14} - \hat{H}_{34}\right) + \hat{N}^{(\mathrm{DN})}\left(1 - \hat{\beta}\right)\right]\right|^2\right\}. \tag{48}$$

Ultimately, we propose the MIMO Quasi Deterministic Encoded (MIMO-QD-E) method, a more robust transmitting scheme designed to allow reliable communication also, in the

case of low SNRs. This scheme exploits space-time coding at the transmitter and was inspired by the work in [37].

This method places on the two transmitter ports (2 and 4) the same pair of symbols with swapped order in two consecutive OFDM sub-channels, e.g., sub-channel of index k: (P2:X_2^1, P4:X_4^1); sub-channel $k+1$: (P2:X_4^1, P4:X_2^1); sub-channel $k+2$: (P2:X_2^2, P4:X_4^2); sub-channel $k+3$: (P2:X_4^2, P4:X_2^2). The MIMO-QD-E scheme reduces the overall transmission rate by a factor of two, therefore becoming identical to the SIMO-QD transmission rate.

The respective MIMO-QD-E decoding scheme exploits the symbols displacement, as mentioned earlier, to improve the transmission reliability. Therefore, it retrieves concurrently, two consecutive OFDM sub-channels symbols $(\hat{X}_2, \hat{X}_4)$, exploiting the following ML cost function:

$$\begin{aligned}\left[\hat{X}_2, \hat{X}_4\right]^{\text{QD-E}} = \text{argmin}_{\tilde{X}_2,\tilde{X}_4}\Big\{&\Big|Y_{1a} - \Big(\hat{H}_{12a}\tilde{X}_2 + \hat{H}_{14a}\tilde{X}_4 + \hat{N}_a^{(\text{DN})}\Big)\Big|^2 + \\ &+ \Big|Y_{3a} - \Big(\hat{H}_{32a}\tilde{X}_2 + \hat{H}_{34a}\tilde{X}_4 + \hat{\beta}_a\hat{N}_a^{(\text{DN})}\Big)\Big|^2 + \\ &+ \Big|Y_{1b} - \Big(\hat{H}_{14b}\tilde{X}_2 + \hat{H}_{12b}\tilde{X}_4 + \hat{N}_b^{(\text{DN})}\Big)\Big|^2 + \\ &+ \Big|Y_{3b} - \Big(\hat{H}_{34b}\tilde{X}_2 + \hat{H}_{32b}\tilde{X}_4 + \hat{\beta}_b\hat{N}_b^{(\text{DN})}\Big)\Big|^2\Big\}. \end{aligned} \quad (49)$$

The subscripts $(_a)$ and $(_b)$ correspond to the OFDM sub-channels indexes k and $k+1$.

The QD noise effect is exploited in the MIMO-QD-D, MIMO-QD-L, and MIMO-QD-E methods. Before the decoding procedure, the parameter β, and the CTFs are estimated through a training algorithm, as explained in Section VII-C. However, the noise changes in time, and its QD component needs to be estimated for each symbol during the ML procedure as shown in (46). For instance, substituting Eq. (46) in Eqs. (47), (48) and (49) we obtain ML metrics as a function of the symbols $(\tilde{X}_2, \tilde{X}_4)$, CTFs and $\hat{\beta}$. For example, Eq. (47) becomes as follows:

$$\begin{aligned}\left[\hat{X}_2, \hat{X}_4\right]^{\text{QD-D}} = \text{argmin}_{\tilde{X}_2,\tilde{X}_4}\Big\{&\Big|\hat{\beta}\Big(Y_1 - \tilde{X}_2\hat{H}_{12} - \tilde{X}_4\hat{H}_{14}\Big) + \\ &- \Big(Y_3 - \tilde{X}_2\hat{H}_{32} - \tilde{X}_4\hat{H}_{34}\Big)\Big|^2\Big\}. \end{aligned} \quad (50)$$

The proposed methods can also be used for narrow-band (NB) transmission systems. Specifically, the MIMO-QD-E, in the NB case, can be implemented to subsequent time slots instead of OFDM sub-channels.

C. PARAMETER ESTIMATION

The QD noise mitigation algorithms exploit the estimated CTFs and $\hat{\beta}$ to decode the transmitted signals. The procedure to estimate these quantities is detailed in this section.

A first approach allows to estimate from the received signals Y_1 and Y_3, at first the CTFs and later $\hat{\beta}$. During this procedure, a known training sequence (X_j) is sent from both transmitters 2 and 4. The CTFs are computed via least-squares as follows:

TABLE 1. Complexity of the proposed decoding techniques measured in number of complex operations per OFDM symbol.

	Complex operations
SIMO-QD	(5 mul. + 3 sums)N_oN_c
MIMO-QD-D	(6 mul. + 5 sums)N_oN_c + (7 mul. + 7 sums)N_oN_c
MIMO-QD-L	(6 mul. + 5 sums)N_oN_c + (8 mul. + 13 sums)N_oN_c
MIMO-QD-E	2(6 mul. + 5 sums)N_oN_c + (14 mul. + 15 sums)N_oN_c

$$\begin{aligned}\hat{H}_{ij} &= \mathbb{E}\big[Y_i/X_j\big], \\ i &= \{1,3\}; j = \{2,4\}. \end{aligned} \quad (51)$$

while, the noise deterministic component is derived subtracting the channel effect from the received signals Y_1 and Y_3. Thus,

$$\hat{\beta} = \mathbb{E}\left[\frac{Y_3 - \hat{H}_{32}X_2 - \hat{H}_{34}X_4}{Y_1 - \hat{H}_{12}X_2 - \hat{H}_{14}X_4}\right], \quad (52)$$

where $\hat{\beta}$ is obtained computing Eq. (52) on several realizations of the received signals.

A second approach estimates β during the silent transmission period. While the CTFs are successively estimated when the training symbols are received. Then, β is estimated as follows:

$$\hat{\beta} = \mathbb{E}\big[Y_3/Y_1\big]. \quad (53)$$

In our investigations, the second method has proved to be more effective (i.e., four silent symbols are sufficient to estimate β). However, another possibility is to use both approaches alternatively, averaging the results. This allows to reduce the number of silent symbols and therefore increase the throughput. For example, we might perform the first estimation of β in one silent symbol before the beginning of the communication. Then, the estimation of β is refined during the communication procedures exploiting the relation (52).

The decoding techniques come along with a computational cost which is not always negligible. Table 1 shows the complexity of the proposed techniques measured in number of complex operations per OFDM symbol (additions and multiplications). N_o indicates the number of OFDM symbols, while N_c is the number of constellation symbols. For example, in BPSK, N_c=2, and in 4PSK it is equal to four. Moreover, the cost of searching the minimum argument necessary for the ML technique is not considered in Tab. 1.

D. RESULTS

The dataset of measurements is described in Appendix B and it includes in-home/office MCO scenarios. The QD model parameter $\hat{\beta}$ is estimated every 10ms as explained in Section VII-C (second-approach). The comparison of the decoding techniques is shown in Fig. 16, where the SIMO and MIMO average Bit Error Bate (BER) as a function of the Signal to Noise Ratio (SNR) of the different decoding

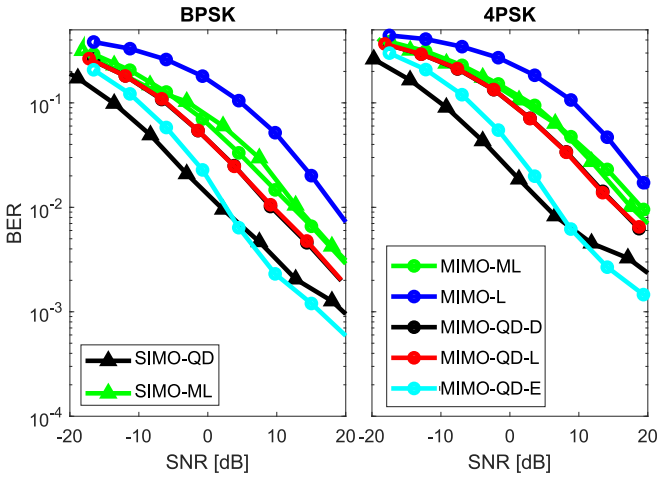

FIGURE 16. Average BER for SIMO-ML and SIMO-QD and MIMO-ML, MIMO-L, MIMO-QD-D, MIMO-QD-L, MIMO-QD-E decoding algorithms for BPSK and 4PSK modulations.

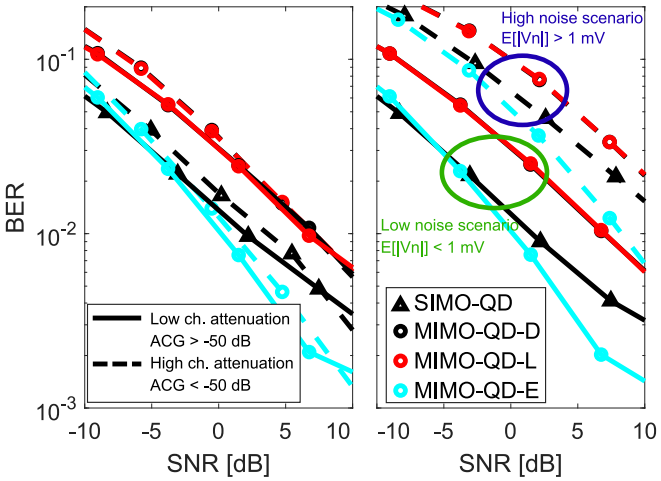

FIGURE 17. BER comparison between QD methods in different scenarios. On the left the comparison between BER results for scenarios with low (non-dashed line) and high (dashed line) average channel gain (ACG). On the right the comparison between scenarios with high (dashed line) and low (non-dashed line) noise magnitude.

techniques are presented for both BPSK and 4PSK modulations. The SNR is defined as the ratio in dB scale of signal power to the noise power at the receiver. In general, the techniques that exploit the QD noise (e.g., SIMO-QD, MIMO-QD-D and MIMO-QD-L) achieve better results, on average by more than 5 dB of SNR, than the classical (e.g., SIMO-ML, MIMO-L and MIMO-ML) methods. The gain of the proposed decoding methods derives from the noise cancellation ability enabled by the estimation of the MCO DN component. Graphically, this is shown by the shift-down of the BER vs. SNR curves. The SIMO-QD decoding technique shows the best performance for low SNR values. In contrast, the MIMO-QD-E obtains the best performance for high SNRs. The SIMO-ML and MIMO-ML as expected show similar results because they exploit the classic decoding technique without considering the QD noise effect. The MIMO-L shows the worst results, as expected from the considerations on the CTFs inversion problems in Section III.

To dig further and evaluate how performance changes in low attenuated channels or in high noisy channels, Fig. 17 shows the BER for the QD decoding methods in the case of BPSK modulation in four different scenarios. From the dataset, the measurements are partitioned into four classes by grouping channels according to the average channel gain (ACG) or noise voltage magnitude (Vn). The channels with ACG < -50dB have been grouped in the scenario named high channel attenuation. While channels with ACG ≥ -50dB have been grouped in the scenario called low channel attenuation. Moreover, the noise voltage magnitude (Vn) has been used as a criterion to group the measurements in high and low noise channel scenarios. Measurements where the noise traces have Vn greater than 1mV are considered in the high noise scenario. While the low noise scenario exhibits noise traces with Vn $<$ 1mV. For each scenario, the BER performance has been numerically evaluated. The figure shows that each decoding algorithm performs similarly in the two ACG classes. This is not the case when we compare the BER performance achieved in high noise scenarios w.r.t. low noise scenarios, where 10dB differences are visible. The high noise class of channels is significantly impacted because it exhibits bursty/impulsive noise that affects the estimation of the parameter β. However, the MIMO-QD-E scheme offers gains and the highest performance among the considered schemes. Further improvements are attainable by estimating β more frequently and adding error correction coding to mitigate the effect of time-variant bursty noise.

VIII. CONCLUSION

The article has presented new methods to characterize and model the DN effect in MCO PLC networks. A bottom-up approach has been used to study the possible factors that cause the deterministic phenomena, considering the noise sources and the front-end circuital structure. A simplified representation of the PLC network and loads has been proposed to highlight the DN component's origin. It has been shown that the deterministic component has a high probability of occurring in the presence of high radiated noise when the CTFs matrix is rank-deficient and with similar MCO channel input impedances.

Moreover, a top-down approach has been exploited to identify a good model that represents the deterministic phenomena. In detail, three statistical metrics to detect determinism in noise time series are proposed and compared: cross-correlation, distance-correlation, and mutual information. The mutual relationship between the correlation and mutual information has been proven effective in defining a threshold that identifies when the PLC noise is mainly deterministic. In addition a linear coefficient ratio has been defined and exploited to model the DN.

Lastly, four decoding algorithms that exploit the QD model to mitigate the noise are detailed, evaluated, and compared

TABLE 2. Conversion formulas.

Comp.	Equations
k_{11}	$(+Z_{11}Z_{22}Z_{44}-Z_{11}Z_{23}Z_{42}-Z_{12}Z_{21}Z_{44}+Z_{12}Z_{23}Z_{41}+Z_{14}Z_{21}Z_{42}-Z_{14}Z_{22}Z_{41}+Z_{11}Z_{22}Z_4^{(g)}-Z_{12}Z_{21}Z_4^{(g)}+Z_{11}Z_{44}Z_2^{(g)}-Z_{14}Z_{41}Z_2^{(g)}+Z_{11}Z_2^{(g)}Z_4^{(g)})/(Z_{22}Z_{44}-Z_{23}Z_{42}+Z_{22}Z_4^{(g)}+Z_{44}Z_2^{(g)}+Z_2^{(g)}Z_4^{(g)})$
k_{12}	$(-Z_{12}Z_{23}Z_{44}+Z_{12}Z_{23}Z_{43}+Z_{13}Z_{22}Z_{44}-Z_{13}Z_{23}Z_{42}-Z_{14}Z_{22}Z_{43}+Z_{14}Z_{23}Z_{42}-Z_{12}Z_{23}Z_4^{(g)}+Z_{13}Z_{22}Z_4^{(g)}+Z_{13}Z_{44}Z_2^{(g)}-Z_{14}Z_{43}Z_2^{(g)}+Z_{13}Z_2^{(g)}Z_4^{(g)})/(Z_{22}Z_{44}-Z_{23}Z_{42}+Z_{22}Z_4^{(g)}+Z_{44}Z_2^{(g)}+Z_2^{(g)}Z_4^{(g)})$
k_{21}	$(-Z_{21}Z_{32}Z_{44}+Z_{21}Z_{34}Z_{42}+Z_{22}Z_{31}Z_{44}-Z_{22}Z_{34}Z_{41}-Z_{23}Z_{31}Z_{42}+Z_{23}Z_{32}Z_{41}-Z_{21}Z_{32}Z_4^{(g)}+Z_{22}Z_{31}Z_4^{(g)}+Z_{31}Z_{44}Z_2^{(g)}-Z_{34}Z_{41}Z_2^{(g)}+Z_{31}Z_2^{(g)}Z_4^{(g)})/(Z_{22}Z_{44}-Z_{23}Z_{42}+Z_{22}Z_4^{(g)}+Z_{44}Z_2^{(g)}+Z_2^{(g)}Z_4^{(g)})$
k_{22}	$(+Z_{22}Z_{33}Z_{44}-Z_{22}Z_{34}Z_{43}-Z_{23}Z_{32}Z_{44}+Z_{23}Z_{34}Z_{42}+Z_{23}Z_{32}Z_{43}-Z_{23}Z_{33}Z_{42}+Z_{22}Z_{33}Z_4^{(g)}-Z_{23}Z_{32}Z_4^{(g)}+Z_{33}Z_{44}Z_2^{(g)}-Z_{34}Z_{43}Z_2^{(g)}+Z_{33}Z_2^{(g)}Z_4^{(g)})/(Z_{22}Z_{44}-Z_{23}Z_{42}+Z_{22}Z_4^{(g)}+Z_{44}Z_2^{(g)}+Z_2^{(g)}Z_4^{(g)})$
o_{11}	$(+Z_{12}Z_{44}-Z_{14}Z_{42}+Z_{12}Z_4^{(g)})/(Z_{22}Z_{44}-Z_{23}Z_{42}+Z_{22}Z_4^{(g)}+Z_{44}Z_2^{(g)}+Z_2^{(g)}Z_4^{(g)})$
o_{12}	$(+Z_{14}Z_{22}-Z_{12}Z_{23}+Z_{14}Z_2^{(g)})/(Z_{22}Z_{44}-Z_{23}Z_{42}+Z_{22}Z_4^{(g)}+Z_{44}Z_2^{(g)}+Z_2^{(g)}Z_4^{(g)})$
o_{21}	$(+Z_{32}Z_{44}-Z_{34}Z_{42}+Z_{32}Z_4^{(g)})/(Z_{22}Z_{44}-Z_{23}Z_{42}+Z_{22}Z_4^{(g)}+Z_{44}Z_2^{(g)}+Z_2^{(g)}Z_4^{(g)})$
o_{22}	$(+Z_{22}Z_{34}-Z_{23}Z_{32}+Z_{34}Z_2^{(g)})/(Z_{22}Z_{44}-Z_{23}Z_{42}+Z_{22}Z_4^{(g)}+Z_{44}Z_2^{(g)}+Z_2^{(g)}Z_4^{(g)})$

with classical decoding methods for SIMO and MIMO transmission systems. The proposed algorithms show significant gain w.r.t. the classical decoding algorithms. The mitigation algorithms have been evaluated with an emulated transmission system that exploits a dataset of measured noise traces and CTFs.

APPENDIX

A. PLC CHANNEL EQUIVALENT CIRCUIT

The three conductors PLN has been modeled at the local node with a π-network with three equivalent resistors in series with three equivalent generators. This section explains the conversion procedure from a four-port scattering matrix $\mathbf{S}$, for example, acquired by a VNA, to an equivalent π-network circuit with impedances and loads as shown in Fig. 3.

The conversion from the scattering matrix $\mathbf{S}$ to the four by four impedance matrix $\mathbf{Z}$ is done as follows:

$$\mathbf{Z} = (\mathbf{S} + \mathbf{I_d})/(\mathbf{I_d} - \mathbf{S}), \tag{54}$$

where $\mathbf{I_d}$ is the four by four identity matrix. Therefore, the four ports network's currents and voltages are described with the Ohm's low $V = \mathbf{Z}I$. Where V and I are the vectors containing the voltages and currents for each port.

Ports two and four are respectively terminated with generators $V_2^{(g)}$ and $V_4^{(g)}$ in series with loads $Z_2^{(g)}$ and $Z_4^{(g)}$. The following equations specify their relation: $V_2 = V_2^{(g)} - Z_2^{(g)}I_2$, $V_4 = V_4^{(g)} - Z_4^{(g)}I_4$. Where V_2 and V_4 are, respectively, the voltage drops at ports two and four.

The matrix $\mathbf{Z}$ is then transformed to an hybrid matrix $\mathbf{U} = [\mathbf{K}, \mathbf{O}]$ with the following structure:

$$\begin{aligned} V_1 &= k_{11}I_1 + k_{12}I_3 + o_{11}V_2^{(g)} + o_{12}V_4^{(g)}, \\ V_3 &= k_{21}I_1 + k_{22}I_3 + o_{21}V_2^{(g)} + o_{22}V_4^{(g)}. \end{aligned} \tag{55}$$

The dependent variables are the generators' voltages and the currents at ports two and four. Table 2, contains the conversion formulas from the impedance matrix factors to the sub-matrices $\mathbf{K}$ and $\mathbf{O}$.

The $\mathbf{K}$ sub-matrix parameters are converted to describe a π-impedance network with the following equations:

$$\begin{aligned} Z_1^{(p)} &= \frac{k_{11}k_{22} - k_{12}^2}{k_{22} - k_{12}}, \\ Z_3^{(p)} &= \frac{k_{11}k_{22} - k_{12}^2}{k_{11} - k_{12}}, \\ Z_{13}^{(p)} &= \frac{k_{11}k_{22} - k_{12}^2}{k_{12}}, \end{aligned} \tag{56}$$

where $Z_1^{(p)}$, $Z_3^{(p)}$ and $Z_{13}^{(p)}$ are the impedances on the three branches of the π-network, as shown in Fig. 3.

Then, the contribution of the other components has been included in three equivalent generators: $V_1^{(se)}$, $V_3^{(se)}$ and $V_{13}^{(se)}$. The three generators are respectively connected in series to the π impedances $Z_1^{(p)}$, $Z_3^{(p)}$ and $Z_{13}^{(p)}$. Therefore, the equivalent generators $V_1^{(se)}$, $V_3^{(se)}$ and $V_{13}^{(se)}$ are computed as follows:

$$\begin{aligned} V_1^{(se)} &= o_{11}V_2^{(g)} + o_{12}V_4^{(g)}, \\ V_3^{(se)} &= o_{21}V_2^{(g)} + o_{22}V_4^{(g)}, \\ V_{13}^{(se)} &= (o_{11} - o_{21})V_2^{(g)} + (o_{12} - o_{22})V_4^{(g)}. \end{aligned} \tag{57}$$

These equivalent components allow to simplify the computation of the multi conductor circuit at the local node. Specifically, has been used to compute the input impedances at the ports 1 and 3 from the equivalent impedances $Z_1^{(p)}$, $Z_3^{(p)}$ and $Z_{13}^{(p)}$ as follows:

$$\begin{aligned} Z_{in1} &= \frac{V_1^{(p)}}{I_1} = Z_1^{(p)} // \left(Z_{13}^{(p)} + \left(Z_3^{(p)} // Z_3^{(g)}\right)\right), \\ Z_{in3} &= \frac{V_3^{(p)}}{I_3} = Z_3^{(p)} // \left(Z_{13}^{(p)} + \left(Z_1^{(p)} // Z_1^{(g)}\right)\right), \end{aligned} \tag{58}$$

where the symbol // defines the parallel operation between two impedances $Z_a // Z_b = Z_a Z_b/(Z_a + Z_b)$.

B. NOISE AND CTF DATASETS

Multiple experimental measurement campaigns have been carried out to characterize PLC noise and CTFs. The

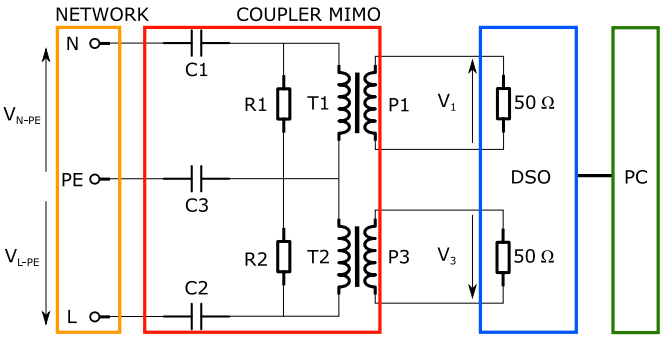

FIGURE 18. Basic schematic of the capacitive coupling circuit used in the measurement campaign. The coupler is designed for three-conductors power line networks. Two ports (and their respective voltage V_1 and V_3) are available for the communication.

diversity of noise sources and behaviors required to analyze the noise traces in different scenarios and measurement setups. The measurements have been performed mainly in the laboratories and offices at the Klagenfurt University (Austria). Where, the following two datasets were created:

- Dataset 1: dataset of PLC noise (Noise traces in the time-domain, with a duration of 20ms, have been acquired concurrently from the two MCO ports. Several traces have been acquired from more than 100 different PLC outlets).
- Dataset 2: dataset of PLC CTFs (The MIMO 2x2 CTFs are acquired in the frequency domain, with a resolution of 75kHz, in the frequency band from 1 to 100MHz. Several CTFs have been acquired from more than 100 different PLC outlets).

The datasets mentioned above have been used in this article to characterize the deterministic effects of the noise. The considered spectrum has been up to 50 MHz. A sample of the data set has been rendered available in the IEEE DataPort repository [38]. The measurement of CTFs has been conducted with a Vector Network Analyzer (Rohde and Schwarz ZNB 8). Whereas, the noise traces have been acquired with a Digital Storage Oscilloscope (LeCroy Wave Runner). Both instruments are designed to acquire simultaneously four signal ports. The DSO can acquire the four channels concurrently, while the VNA schedules the acquisition of the four channels in consecutive time intervals. This instrumentation allowed to characterize the 2x2 MIMO channels and noise.

A coupling circuit has been used as the interface between the PLC network and the instrumentation, as shown in Fig. 18. The coupling circuit filters out the low-frequency signal and preserves the PLC broadband spectrum. Moreover, it serves as galvanic protection for the connected instruments.

The DSO and VNA have been synchronized to the mains through a trigger device with a period (T) of 20ms, i.e., Europe's mains period. The DSO input impedances have been set equal to 50Ω. The noise voltage traces have duration of 20ms and been acquired with sampling frequency of 100Msamples/second. The vector network analyzer has been set to acquire the scattering matrix of the four ports under analysis. The frequency resolution is 75kHz; thus, 1320 points are available between 1 and 100MHz. Port 1 and port 3 represent the local node and have been respectively connected to P1 and P3 of the coupler device. While ports 2 and 4 represent the remote node. Eventually, the scattering matrix has been converted to the CTF matrix. The voltages at the local node have been represented as follows:

$$\begin{aligned} V_1 &= H_{12}V_2 + H_{14}V_4, \\ V_3 &= H_{32}V_2 + H_{34}V_4. \end{aligned} \tag{59}$$

While the voltages at the remote node have been represented as follows:

$$\begin{aligned} V_2 &= H_{21}V_1 + H_{23}V_3, \\ V_4 &= H_{41}V_1 + H_{43}V_3. \end{aligned} \tag{60}$$

The CTF and noise measurements have been done consecutively to acquire as much as possible the same condition of the network for both channels and noise. Considering measurements at the same outlet ports, only the time to connect the different instruments passed (about three minutes) between the noise and CTFs data acquisition. The datasets contain the data acquired from more than 100 different PLC outlets, sampled at least two different times for each of them.

The measurement procedure is controlled by a MATLAB script that includes the setup information, data storage capabilities, and post-processing algorithms.

REFERENCES

[1] L. Lampe, A. M. Tonello, and T. G. Swart, Eds., *Power Line Communications: Principles, Standards and Applications From Multimedia to Smart Grid*. Hoboken, NJ, USA: Wiley, 2016.

[2] C. Cano, A. Pittolo, D. Malone, L. Lampe, A. M. Tonello, and A. G. Dabak, "State of the art in power line communications: From the applications to the medium," *IEEE J. Sel. Areas Commun.*, vol. 34, no. 7, pp. 1935–1952, Jul. 2016.

[3] A. M. Tonello and F. Pecile, "Synchronization for multiuser wide band impulse modulation systems in power line channels with unstationary noise," in *Proc. IEEE Int. Symp. Power Line Commun. Appl.*, Mar. 2007, pp. 150–154.

[4] L. D. Bert, P. Caldera, D. Schwingshackl, and A. M. Tonello, "On noise modeling for power line communications," in *Proc. IEEE Int. Symp. Power Line Communi. Appl.*, Apr. 2011, pp. 283–288.

[5] A. Pittolo, A. M. Tonello, and F. Versolatto, "Performance of MIMO PLC in measured channels affected by correlated noise," in *Proc. 18th IEEE Int. Symp. Power Line Commun. Appl.*, Glasgow, U.K., Mar. 2014, pp. 261–265.

[6] P. Pagani, R. Hashmat, A. Schwager, D. Schneider, and W. Baschlin, "European MIMO PLC field measurements: Noise analysis," in *Proc. IEEE Int. Symp. Power Line Commun. Appl.*, Mar. 2012, pp. 310–315.

[7] M. Antoniali, F. Versolatto, and A. M. Tonello, "An experimental characterization of the PLC noise at the source," *IEEE Trans. Power Del.*, vol. 31, no. 3, pp. 1068–1075, Jun. 2016.

[8] F. Passerini and A. M. Tonello, "Smart grid monitoring using power line modems: Effect of anomalies on signal propagation," *IEEE Access*, vol. 7, pp. 27302–27312, 2019.

[9] F. Passerini and A. M. Tonello, "Analysis of high-frequency impedance measurement techniques for power line network sensing," *IEEE Sensors J.*, vol. 17, no. 23, pp. 7630–7640, Dec. 2017.

[10] J. A. Cortés, J. A. Corchado, F. J. Cañete, and L. Díez, "Analysis and exploitation of the noise correlation in MIMO power line communications in the FM band," *IEEE Commun. Lett.*, vol. 22, no. 3, pp. 566–569, Mar. 2018.

[11] G. Prasad and L. Lampe, "Full-duplex power line communications: Design and applications from multimedia to smart grid," *IEEE Commun. Mag.*, vol. 58, no. 2, pp. 106–112, Feb. 2020.
[12] F. Passerini and A. M. Tonello, "Analog full-duplex amplify-and-forward relay for power line communication networks," *IEEE Commun. Lett.*, vol. 23, no. 4, pp. 676–679, Apr. 2019.
[13] G. Hallak, C. Nieß, and G. Bumiller, "Accurate low access impedance measurements with separated load impedance measurements on the power-line network," *IEEE Trans. Instrum. Meas.*, vol. 67, no. 10, pp. 2282–2293, Oct. 2018.
[14] F. Passerini and A. M. Tonello, "Power line fault detection and localization using high frequency impedance measurement," in *Proc. IEEE Int. Symp. Power Line Commun. Appl. (ISPLC)*, Apr. 2017, pp. 1–5.
[15] V. Degardin, M. Lienard, A. Zeddam, F. Gauthier, and P. Degauquel, "Classification and characterization of impulsive noise on indoor powerline used for data communications," *IEEE Trans. Consumer Electron.*, vol. 48, no. 4, pp. 913–918, Nov. 2002.
[16] M. Nassar, A. Dabak, I. H. Kim, T. Pande, and B. L. Evans, "Cyclostationary noise modeling in narrowband powerline communication for smart grid applications," in *Proc. IEEE Int. Conf. Acoust. Speech Signal Process. (ICASSP)*, Mar. 2012, pp. 3089–3092.
[17] C. Kaiser, N. Otterbach, and K. Dostert, "Spectral correlation analysis of narrowband power line noise," in *Proc. IEEE Int. Symp. Power Line Commun. Appl. (ISPLC)*, Apr. 2017, pp. 1–6.
[18] M. Zimmermann and K. Dostert, "Analysis and modeling of impulsive noise in broad-band powerline communications," *IEEE Trans. Electromagn. Compat.*, vol. 44, no. 1, pp. 249–258, Feb. 2002.
[19] J. Lin, M. Nassar, and B. L. Evans, "Impulsive noise mitigation in powerline communications using sparse Bayesian learning," *IEEE J. Sel. Areas Commun.*, vol. 31, no. 7, pp. 1172–1183, Jul. 2013.
[20] A. M. Tonello, N. A. Letizia, D. Righini, and F. Marcuzzi, "Machine learning tips and tricks for power line communications," *IEEE Access*, vol. 7, pp. 82434–82452, 2019.
[21] N. A. Letizia, A. M. Tonello, and D. Righini, "Learning to synthesize noise: The multiple conductor power line case," in *Proc. IEEE Int. Symp. Power Line Commun. Appl. (ISPLC)*, May 2020, pp. 1–6.
[22] O. G. Hooijen, "A channel model for the residential power circuit used as a digital communications medium," *IEEE Trans. Electromagn. Compat.*, vol. 40, no. 4, pp. 331–336, Nov. 1998.
[23] B. Han, V. Stoica, C. Kaiser, N. Otterbach, and K. Dostert, "Noise characterization and emulation for low-voltage power line channels across narrowband and broadband," *Digit. Signal Process.*, vol. 69, pp. 259–274, Oct. 2017.
[24] M. Katayama, T. Yamazato, and H. Okada, "A mathematical model of noise in narrowband power line communication systems," *IEEE J. Sel. Areas Commun.*, vol. 24, no. 7, pp. 1267–1276, Jul. 2006.
[25] D. Righini and A. M. Tonello, "Automatic clustering of noise in multi-conductor narrow band PLC channels," in *Proc. IEEE Int. Symp. Power Line Commun. Appl. (ISPLC)*, Apr. 2019, pp. 1–6.
[26] J. A. Cortés, L. Díez, F. J. Cañete, and J. J. Sánchez-Martínez, "Analysis of the indoor broadband power-line noise scenario," *IEEE Trans. Electromagn. Compat.*, vol. 52, no. 4, pp. 849–858, Nov. 2010.
[27] B. Han, C. Kaiser, and K. Dostert, "A novel approach of canceling cyclostationary noise in low-voltage power line communications," in *Proc. IEEE Int. Conf. Commun. (ICC)*, Jun. 2015, pp. 734–739.
[28] D. Middleton, "Procedures for determining the parameters of the first-order canonical models of class A and class B electromagnetic interference," *IEEE Trans. Electromagn. Compat.*, vol. EMC-21, no. 3, pp. 190–208, Aug. 1979.
[29] D. Righini and A. M. Tonello, "Noise determinism in multi-conductor narrow band PLC channels," in *Proc. IEEE Int. Symp. Power Line Commun. Appl. (ISPLC)*, Apr. 2018, pp. 1–6.
[30] D. Righini, F. Passerini, and A. M. Tonello, "Modeling transmission and radiation effects when exploiting power line networks for communication," *IEEE Trans. Electromagn. Compat.*, vol. 60, no. 1, pp. 59–67, Feb. 2018.
[31] A. Vukicevic, M. Rubinstein, F. Rachidi, and J.-L. Bermudez, "On the mechanisms of differential-mode to common-mode conversion in the broadband over power line (BPL) frequency band," in *Proc. 17th Int. Zurich Symp. Electromagn. Compat.*, 2006, pp. 658–661.
[32] M. Elgenedy, M. Sayed, N. Al-Dhahir, and R. C. Chabaan, "Cyclostationary noise mitigation for SIMO powerline communications," *IEEE Access*, vol. 6, pp. 5460–5484, 2018.
[33] G. J. Székely, M. L. Rizzo, and N. K. Bakirov, "Measuring and testing dependence by correlation of distances," *Ann. Stat.*, vol. 35, no. 6, pp. 2769–2794, Dec. 2007.
[34] A. Kraskov, H. Stögbauer, and P. Grassberger, "Estimating mutual information," *Phys. Rev. E, Stat. Phys. Plasmas Fluids Relat. Interdiscip. Top.*, vol. 69, Jun. 2004, Art. no. 066138.
[35] R. Steuer, J. Kurths, C. O. Daub, J. Weise, and J. Selbig, "The mutual information: Detecting and evaluating dependencies between variables," *Bioinformatics*, vol. 18, pp. S231–S240, Oct. 2002.
[36] C. M. Bishop, *Pattern Recognition and Machine Learning (Information Science and Statistics)*, 1st ed. Heidelberg, Germany: Springer, 2007.
[37] R. Y. Mesleh, H. Haas, S. Sinanovic, C. W. Ahn, and S. Yun, "Spatial modulation," *IEEE Trans. Veh. Technol.*, vol. 57, no. 4, pp. 2228–2241, Jul. 2008.
[38] D. Righini and A. M. Tonello. (2021). *Multi-Conductor Power Line Communication CTF, Impendance, and Noise*. [Online]. Available: https://ieee-dataport.org/open-access/multi-conductor-power-line-communication-ctf-impendance-and-noise

DAVIDE RIGHINI (Student Member, IEEE) received the Laurea Magistrale degree in electronic engineering from the University of Udine, Italy, in 2016. He is currently a University Assistant with the NES Institute, University of Klagenfurt, Austria. His research interests include modeling, characterization and measurement of cyber physical systems including sensor, and communication technologies.

ANDREA M. TONELLO (Senior Member, IEEE) received the Laurea degree (*summa cum laude*) in electrical engineering and the Doctor of Research degree in electronics and telecommunications from the University of Padua, Padua, Italy, in 1996 and 2002, respectively. From 1997 to 2002, he was with Bell Labs-Lucent Technologies, Whippany, NJ, USA, first as a Member of the Technical Staff. He was then promoted to Technical Manager and appointed as the Managing Director of the Bell Labs, Italy. In 2003, he joined the University of Udine, Udine, Italy, where he became an Aggregate Professor in 2005, and an Associate Professor in 2014. He is currently a Professor with the Chair of Embedded Communication Systems, University of Klagenfurt, Klagenfurt, Austria. He received several awards, including the Bell Labs Recognition of Excellence Award in 1999, the Distinguished Visiting Fellowship from the Royal Academy of Engineering, U.K., in 2010, the IEEE Distinguished Lecturer Award from VTS (2011–2015) and from COMSOC (2018–2019), the Italian Full Professor Habilitation in 2013, the Chair of Excellence from Carlos III Universidad, Madrid in 2019 and 2020. He was also a co-recipient of nine best paper awards. He was the general chair or a TPC co-chair of several conferences. He was the Chair of the IEEE COMSOC Technical Committee (TC) on Power Line Communications (2014–2018) and he is currently the Chair of the TC on Smart Grid Communications. He also serves as the Director of Industry Outreach of IEEE COMSOC for the term 2020–2021. He serves/ed as Associate Editor of several journals, including IEEE TRANSACTIONS ON VEHICULAR TECHNOLOGY, IEEE TRANSACTIONS ON COMMUNICATIONS, IEEE ACCESS, and *IET Smart Grid*.